

INTERGALACTIC PROPAGATION OF UHE COSMIC RAYS

Abraham Achterberg^{1,2}, Yves Gallant^{1,3}, Colin A. Norman^{4,5} and Donald B. Melrose⁶

¹*Astronomical Institute, Utrecht University, P.O. box 80.000, 3508 TA Utrecht, The Netherlands*

²*Center for High Energy Astrophysics, Kruislaan 403, 1098 SJ Amsterdam, The Netherlands*

³*Dublin Institute for Advanced Studies, 5 Merrion Square, Dublin 2, Republic of Ireland*

⁴*Department of Physics and Astronomy, Johns Hopkins University, Homewood campus, Baltimore MD 21218*

⁵*Space Telescope Science Institute, 3700 San Martin Drive, Baltimore, MD 21218*

⁶*Research Center for Theoretical Astrophysics, School of Physics, University of Sydney, NSW 2006, Australia*

29 April 2024

ABSTRACT

We discuss the intergalactic propagation of ultra-high-energy cosmic rays (UHECRs) with energies $E \gtrsim 10^{18.5}$ eV. We consider the propagation of UHECRs under the influence of the energy-dependent deflection by a weak random magnetic field in the intergalactic medium and energy losses by photo-pion and pair production. We calculate arrival spectra taking full account of the kinematics of photo-pion production and the Poisson statistics of the photo-pion interaction rate.

We give estimates for the deflection of UHECRs from the line of sight to the source, time delays with respect to photons from the same source, arrival spectra and source statistics. These estimates are confirmed by numerical simulations of the propagation in energy evolution of UHECRs. These simulations demonstrate that the often-used continuous approximation in the treatment of energy losses due to photo-pion production on the cosmic microwave background (CMWB) cannot be justified for UHECRs.

We discuss the implications of these results for the observed flux of particles above the Greisen-Zatsepin-Kuz'min cut-off in the two of the scenarios that have been proposed for the production of these particles: continuous production in the large shock waves associated with powerful radio galaxies, or possibly large-scale structure formation, and the impulsive production at relativistic blast waves associated with cosmological gamma-ray bursts.

Key words: magnetic fields – scattering – gamma-rays: bursts – cosmic rays

1 INTRODUCTION

Recent observations of ultra-high energy cosmic rays (UHECRs) above $10^{18.5}$ eV (Bird et al. , 1994, Yoshida et al. , 1994, Takeda et al. , 1998) suggest that these particles are of extragalactic origin. The indications are threefold:

- (i) The energy spectrum hardens, from $J(E) \propto E^{-3.2 \pm 0.1}$ below $10^{18.5}$ eV to $J(E) \propto E^{-2.8 \pm 0.3}$ above $10^{18.5}$ eV;
- (ii) Arrival directions do not seem to be clustered significantly along the Galactic plane, although there is an indication that they may be clustered along the supergalactic plane for $E > 10^{19.5}$ eV (Hayashida et al. , 1996; Stanev et al. , 1995).
- (iii) There is a suggestion that the composition changes from one dominated by heavy nuclei (iron group) below $10^{18.5}$ eV, as expected for a population of Galactic origin, to

one dominated by light nuclei or even protons above $10^{18.5}$ eV;

At these energies the deflection of UHECRs in the $\sim \mu\text{G}$ Galactic magnetic fields is too small to randomise flight directions within the Galaxy. In terms of the typical gyration radius of a particle with energy E and charge $q = Ze$ and pitch angle i , $\rho_G = r_g(E) \sin i$ with $r_g(E) \equiv E/ZeB$, the deflection angle $\Delta\theta$ inside the Galactic disk of size $d \sim 10$ kpc is of order

$$\Delta\theta \simeq \frac{d}{r_g(E)} = 6^\circ (ZB_{\mu\text{G}}/E_{20}) , \quad (1)$$

with $E_{20} \equiv E/(10^{20} \text{ eV})$. In practice, it will be much less due to the inclination of the particle orbit with respect to the disk plane and the fact that the Galactic magnetic field is strongly turbulent on kpc scales (for a review: Zweibel & Heiles, 1997), and will not act coherently over the whole

disk. Therefore, an origin of UHECRs within the Galactic disk should lead to a significant clustering of arrival directions around the Galactic plane, unless the sources are in an extensive halo around the Galaxy.

From a theoretical point of view, the fundamental limit on the maximum energy attainable in any electrodynamic acceleration mechanism relying on bulk plasma motions (i.e. waves or shocks) is (Norman, Melrose & Achterberg, 1995; Gallant & Achterberg, 1999)

$$E_{\max} \sim Ze\Gamma_s\beta_s BR_s. \quad (2)$$

Here $\beta_s = V/c$ is the wave or bulk velocity in units of the speed of light, $\Gamma_s = (1 - \beta_s^2)^{-1/2}$ is the associated Lorentz factor, B is the magnetic field strength and R_s is the linear size of the source. This limit strongly constrains any model for the production of UHECRs (Norman, Melrose & Achterberg, 1995). Galactic sources, with the possible exception of radio pulsars, seem to be excluded. The value of E_{\max} for these source falls well below the UHECR energy range.

For the above reasons, most theoretical discussions of the origin of these particles have centered on extragalactic sources. Leaving aside for the moment the more exotic models involving some fundamental particle or its decay products (e.g. Farrar & Biermann, 1998) or quantum-mechanical topological defects (such as superconducting strings, e.g. Sigl et al., 1994), there are two major classes of models describing the production of UHECRs:

- **Continuous production** of UHECRs in the kpc-scale shocks associated with the jets of powerful Fanaroff-Riley class II radio galaxies (Rachen & Biermann, 1993; Norman, Melrose & Achterberg, 1995), or in shocks associated with ongoing large-scale structure formation in clusters of galaxies (Norman, Melrose & Achterberg, 1995; Kang, Ryu & Jones, 1996; Kang, Rachen & Biermann, 1997);

- **Impulsive production** in the same sources responsible for gamma-ray bursts (Waxman, 1995a; Vietri, 1995; Milgrom & Usov, 1995). This possibility has been proposed on the basis of a striking coincidence: the typical UHECR energy flux above 10^{19} eV, and the typical gamma-ray flux from gamma-ray bursters in the cosmological scenario (Paczynski, 1986) is roughly the same. The recent identification of optical counterparts for several gamma-ray bursts (van Paradijs et al., 1997; Djorgovski et al., 1997; Metzger et al., 1997) seems to indicate that they indeed occur at cosmological distances, and not in an extended halo around our own galaxy as had also been proposed.

A recent review of the various issues involved in the production and propagation of UHECRs can be found in Biermann (1995).

A complication in all these models is the limited volume in the local universe, corresponding to a typical radius $D_{\max} \sim 50$ Mpc, from which UHECRs above $10^{19.5}$ eV must originate if they are indeed protons or light nuclei, and not some exotic particle. Interaction between photons of the Cosmic Microwave Background (CMWB) and UHECRs leads to photo-pion production, e.g. $p + \gamma \rightarrow p + \pi$'s. This process strongly degrades the energy of particles above the Greisen-Zatsepin-Kuz'min cut-off energy $E_c \simeq 10^{19.5}$ eV (Greisen, 1966; Zatsepin & Kuz'min, 1966) with a typical loss length of about 20-30 Mpc above 10^{20} eV.

The observation in 1991 with the Fly's Eye detector of a particle with an energy of $E \simeq 3 \times 10^{20}$ eV (Bird et al., 1995), and more recently of six events above 10^{20} eV with the Akeno Giant Air Shower Array (Takeda et al., 1998), all well above the GZK cut-off, suggests either relatively close-by but unidentified continuous sources ($D < 50$ Mpc, e.g. Elbert & Sommers, 1995), or the scenario where particles are produced impulsively and arrive with a strongly energy-dependent delay with respect to photons due to scattering on weak intergalactic magnetic fields (Waxman, 1995a,b; Waxman & Coppi, 1996; Miralda-Escudé & Waxman, 1996; Waxman & Miralda-Escudé, 1996). In the latter case, an identification of the source in other wavelength bands is not to be expected if the delay is large enough. As we will show, for reasonable values of the magnetic field strength in the intergalactic medium, the delay of UHECRs with respect to photons could be as large as $10^3 - 10^5$ years.

In this paper we will not address the production mechanism of UHECRs. Rather we will concentrate on the propagation of these particles in the intergalactic medium (IGM) under the influence of weak IGM magnetic fields and their interaction with the cosmic microwave background. Scattering on IGM magnetic fields leads to diffusion in the flight direction of UHECR particles, which induces a time delay with respect to photons emitted simultaneously at the source (e.g. Waxman, 1995; Miralda-Escudé & Waxman, 1996). The latter effect is especially important in GRB models of UHECR production, where a time delay between the primary gamma ray photons and 'secondary' UHECRs produced concurrently may yield a strong observational constraint on the strength of the IGM magnetic field. Both the time delay and rms deflection are strong functions of particle energy, $t_{\text{del}} \propto E^{-2}$ and $\alpha_{\text{rms}} \propto E^{-1}$, so that losses incurred by UHECR particles due to their interaction with the CMWB (pion production, and pair production below 10^{19} eV) strongly influence particle propagation.

In Section 2 we systematically derive the relevant equations for the propagation of UHECRs in a weak, random intergalactic magnetic field. In Section 3, the precise form of the energy losses is considered. We re-examine the treatment of energy losses of UHECRs and show that a continuous approximation in terms of the mean energy loss is not a good approximation for particles above 10^{19} eV. In particular we will show that the correct treatment of the Poisson statistics of photon-UHECR encounters leads to a significant high-energy tail in the spectrum for sources closer than ~ 50 Mpc. In Section 4 we present numerical simulations of cosmic-ray propagation. The observational consequences in terms of the different UHECR production scenarios are discussed in Section 5. Conclusions are presented in Section 6.

2 UHECR PROPAGATION IN INTERGALACTIC FIELDS

In the tenuous intergalactic medium (IGM), magnetic fields are responsible for the deflection of UHECRs. Direct measurements of the IGM field strength *outside* clusters are not available. Observational limits (Kronberg, 1996) can be placed on the ordered (large-scale) component $\langle B \rangle_{\text{IGM}}$ and the amplitude B_r of the random component of the inter-

galactic magnetic field. The random component is assumed to have a coherence length $\ell_{\text{coh}} \simeq 1$ Mpc. These limits are:

$$\langle B \rangle_{\text{IGM}} \lesssim 10^{-11} \text{ G}, \quad (3)$$

$$B_r \lesssim 10^{-9} \text{ G}.$$

The field strengths within clusters of galaxies can be much larger, $B \simeq 10^{-7} - 10^{-6}$ G.

The typical gyration radius of an ultra-relativistic cosmic ray particle with charge $q = Ze$ and energy E in a magnetic field B is

$$r_g(E) \simeq \frac{E}{ZeB} \simeq 0.1 \left(\frac{E_{20}}{ZB_{-9}} \right) \text{ Gpc}. \quad (4)$$

Here we have defined

$$E_{20} \equiv \frac{E}{10^{20} \text{ eV}}, \quad B_{-9} \equiv \frac{B}{10^{-9} \text{ G}}. \quad (5)$$

These estimates imply that the turning angle of UHECR particles in the average field $\langle B \rangle_{\text{IGM}}$ over a distance D will be

$$\theta \simeq \frac{D}{r_g(E)} \simeq 0.53^\circ \frac{Z D_2}{E_{20}} \left(\frac{\langle B \rangle_{\text{IGM}}}{10^{-11} \text{ G}} \right). \quad (6)$$

In this expression we defined $D_2 \equiv D/(100 \text{ Mpc})$. This estimate assumes a uniform field so it is actually an upper limit.

The time delay with respect to ballistic propagation follows from expanding the relationship between the path length ℓ along the circular orbit of a charged particle with gyration radius $r_g(E)$ and the linear distance D travelled. It equals, for $\ell \ll r_g(E)$,

$$t_{\text{delay}} \simeq \frac{D^3}{24c r_g^2(E)} \simeq 1200 \frac{Z^2 D_2^3}{E_{20}^2} \left(\frac{\langle B \rangle_{\text{IGM}}}{10^{-11} \text{ G}} \right)^2 \text{ yr}. \quad (7)$$

In what follows, we will assume that the influence of the mean field on UHECR propagation can be neglected with respect to the action of the random field component. We do not believe that a the intergalactic magnetic field will be uniform on scales exceeding ~ 10 Mpc, the typical scale associated the large-scale structure of our Universe. In that case, the contribution of the large-scale field to the delay would be measured in terms of a few years around 10^{20} eV.

2.1 Small-angle scattering by random fields

The equations of motion for an ultra-relativistic particle with charge Ze and energy E in a quasi-static magnetic field can be written as

$$\frac{d\mathbf{x}}{ds} = \hat{\mathbf{n}}, \quad \frac{d\hat{\mathbf{n}}}{ds} = \left(\frac{Ze|\mathbf{B}|}{E} \right) \hat{\mathbf{n}} \times \hat{\mathbf{b}}. \quad (8)$$

Here $s \equiv ct$ is the path length along the orbit, $\hat{\mathbf{n}} \equiv (n_1, n_2, n_3)$ is the unit vector along the direction of flight and $\hat{\mathbf{b}} \equiv (b_1, b_2, b_3)$ is the unit vector along the magnetic field. For simplicity we will assume that the magnetic field has a uniform amplitude B_r and a random (isotropic) direction distribution so that

$$|\mathbf{B}| = B_r, \quad \langle \langle b_i \rangle \rangle = 0, \quad \langle \langle b_i b_j \rangle \rangle = \frac{1}{3} \delta_{ij}. \quad (9)$$

Here the double brackets $\langle \langle \dots \rangle \rangle$ denote an ensemble average. This assumption is equivalent to a collection of randomly oriented cells with a uniform value of the magnetic field strength. The quasi-static treatment of the magnetic field corresponds to the requirement

$$|(\hat{\mathbf{n}} \cdot \nabla) \hat{\mathbf{b}}| \gg \left| \frac{1}{c} \frac{\partial \hat{\mathbf{b}}}{\partial t} \right|, \quad (10)$$

which is always satisfied as the bulk (turbulent) velocity in the IGM is much less than the speed of light.

The equation of motion for $\hat{\mathbf{n}}$ can be written in component form as:

$$\frac{dn_i}{ds} = \frac{\epsilon_{ijk} n_j b_k}{r_g(E)}, \quad (11)$$

with $r_g(E) \equiv E/ZeB_r$ and ϵ_{ijk} the totally anti-symmetric Levi-Cevita tensor. The summation convention is used here and below. Magnetic scattering leads to diffusion of the flight direction $\hat{\mathbf{n}}$. The corresponding diffusion coefficient,

$$\mathcal{D}_{ij} \equiv \frac{\langle \Delta n_i \Delta n_j \rangle}{2\Delta s}, \quad (12)$$

follows from the Kubo-Taylor formula (Taylor, 1921; see also: Sturrock, 1994) as

$$\mathcal{D}_{ij} = \frac{1}{r_g^2(E)} \int_0^\infty ds \epsilon_{ikl} n_k(0) \epsilon_{jqr} n_q(s) \langle b_l(0) b_r(\mathbf{x}(s)) \rangle. \quad (13)$$

This diffusion tensor is defined per unit path length, and its components have the dimension $[\text{length}]^{-1}$. If the deflection of the particle incurred in one correlation length is small in the sense that $|\Delta \hat{\mathbf{n}}| \simeq \ell_{\text{coh}}/r_g(E) \ll 1$, the flight direction $\hat{\mathbf{n}}$ may be approximated as constant (ballistic motion) and $n_k(0)n_q(s) \approx n_k(0)n_q(0)$. This essentially corresponds to the well-known *quasi-linear approximation* of wave-particle interactions (e.g. Davidson, 1972). Using Eqn. (9) one has

$$\int_0^\infty ds \langle b_l(0) b_r(\mathbf{x}(s)) \rangle = \frac{\ell_{\text{coh}}}{3} \delta_{lr}. \quad (14)$$

This integral of the two-point correlation $\langle b_l(0) b_r(\mathbf{x}(s)) \rangle$ formally defines the coherence length ℓ_{coh} of the random field. Using the property $\epsilon_{ijk} \epsilon_{ilm} = \delta_{jl} \delta_{km} - \delta_{jm} \delta_{kl}$ of the Levi-Cevita tensor, the resulting diffusion tensor can be written in terms of a scalar diffusion coefficient \mathcal{D}_0 and a projection tensor $\delta_{ij} - n_i n_j$ onto the plane perpendicular to $\hat{\mathbf{n}}$:

$$\mathcal{D}_{ij} = \mathcal{D}_0 (\delta_{ij} - n_i n_j), \quad \mathcal{D}_0 = \frac{\ell_{\text{coh}}}{3r_g^2(E)}. \quad (15)$$

It is easily checked that this diffusion tensor preserves the unit norm $\hat{\mathbf{n}} \cdot \hat{\mathbf{n}} = 1$ since $n_i \mathcal{D}_{ij} n_j = 0$.

The expression for the scalar diffusion coefficient \mathcal{D}_0 can be explained in terms of a simple model. A charged particle crossing a magnetic cell of size $2\ell_{\text{coh}}$ and field strength $|\mathbf{B}| \sim B_r$ turns through an angle

$$\delta\alpha \simeq \frac{2ZeB_\perp \ell_{\text{coh}}}{E}, \quad (16)$$

where B_\perp is the component of the field perpendicular to the particle velocity. Deflections in different cells add up diffusively. After encountering $N \sim s/2\ell_{\text{coh}}$ cells in a distance s particles have turned an angle $\sim \alpha_{\text{rms}}$ corresponding to $\alpha_{\text{rms}}^2 = (s/2\ell_{\text{coh}}) \times \langle \langle (2ZeB_\perp \ell_{\text{coh}}/E)^2 \rangle \rangle$. The associated angle diffusion coefficient is related to scalar diffusion coefficient \mathcal{D}_0 by $\alpha_{\text{rms}}^2 = 4\mathcal{D}_0 s$ (see Eqn. B.17), so one finds:

$$\mathcal{D}_0 \equiv \frac{\alpha_{\text{rms}}^2(s)}{4s} \simeq \frac{1}{3} \frac{\ell_{\text{coh}}}{r_g^2(E)}, \quad (17)$$

Here we used $\langle B_{\perp}^2 \rangle = \frac{2}{3} B_r^2$.

The result (15) carries over to the more general case of scattering by a broad-band spectrum of random magnetic fields. As shown in Appendix A, an isotropic distribution of magnetic fields with a power spectrum $\mathcal{B}(k)$ as a function of wave number, normalised in such a way that

$$B_{\text{rms}}^2 \equiv \langle |B|^2 \rangle = \int_0^\infty dk \mathcal{B}(k), \quad (18)$$

leads to a scalar diffusion coefficient of the form $\mathcal{D}_0 = \ell_{\text{coh}}/3r_g^2(E)$ with $r_g(E) \equiv E/ZeB_{\text{rms}}$ and an effective correlation length equal to

$$\ell_{\text{coh}} = \frac{3\pi}{8B_{\text{rms}}^2} \int_{k_{\text{min}}}^\infty dk \frac{\mathcal{B}(k)}{k}. \quad (19)$$

Here $k_{\text{min}} \sim 2\pi/r_g(E)$ is the smallest wavenumber for which the approximation of using the unperturbed particle trajectory still (marginally) applies.

2.2 Deviation angles and time delays

In this Section, we consider the deviation angle with respect to the line of sight to the source, and the time delay with respect to photons which is accumulated by UHECRs due to small-angle scattering on magnetic cells in the intergalactic medium. Detailed calculations which consider the influence of scattering on the flight direction and position of the particles, can be found in Appendix B.

Scattering leads to a deviation angle between the original direction of flight, taken to be along the z -axis, and the direction of propagation \hat{n} . Defining $\alpha \equiv \cos^{-1}(\hat{n} \cdot \mathbf{e}_z)$ one has after a path length s :

$$\langle \alpha^2 \rangle(s) \simeq 4\mathcal{D}_0 s = \frac{4}{3} \frac{s\ell_{\text{coh}}}{r_g^2(E)}. \quad (20)$$

This differs from the naive estimate, $\alpha^2(s) \sim 2\mathcal{D}_0 s$, by a factor of two due to the effect of dynamical friction.

However, the angle between the line of sight from the source, $\hat{\mathbf{r}} \equiv \mathbf{r}/|\mathbf{r}|$, and the particle flight direction as measured by an observer, defined by $\alpha' \equiv \cos^{-1}(\hat{\mathbf{r}} \cdot \hat{\mathbf{n}})$, will be *less* due to the statistical correlation between the particle position, $\mathbf{r} = (x, y, z)$, and the flight direction $\hat{\mathbf{n}}$. One finds for this angle $\langle \alpha' \rangle = 0$ and $\langle (\alpha')^2 \rangle(s) = \frac{4}{3} \mathcal{D}_0 s$ after a path length s (Eqn. B22). To zeroth order in $\mathcal{D}_0 s$ the linear distance to the source equals $D \simeq s$ (see below). An observer at a distance D will therefore measure a spread of UHECR arrival directions with respect to the local line of sight from the source equal to

$$(\alpha')^2(s \simeq D) = \frac{4}{9} \frac{D\ell_{\text{coh}}}{r_g^2(E)}, \quad (21)$$

which corresponds to an rms value $\alpha_{\text{rms}} = \sqrt{\langle (\alpha')^2 \rangle}$ equal to

$$\alpha_{\text{rms}} \sim 3.5^\circ \left(\frac{ZB_{-9}}{E_{20}} \right) (D_2 \ell_0)^{1/2}. \quad (22)$$

Here we defined $\ell_0 = \ell_{\text{coh}}/(1 \text{ Mpc})$ and $B_{-9} = B_r/(10^{-9} \text{ G})$. This estimate *neglects* the changes in particle energy as it

propagates. Energy losses are important, as we will see in Section 4.

The typical angle between the line of sight to the source from the observer and the original flight direction, $\theta \equiv \cos^{-1}(\hat{\mathbf{r}} \cdot \mathbf{e}_z)$, satisfies $\langle \theta^2(s) \rangle = \frac{4}{3} \mathcal{D}_0 s$, so its rms value satisfies $\theta_{\text{rms}} \simeq \alpha_{\text{rms}}$.

Due to scattering, the path of an individual UHECR is corrugated, leading to a path length increase with respect to ballistic (straight line) propagation. The average scattering-induced arrival time delay with respect to ballistic propagation at the speed of light at distance D , $\langle t_{\text{del}} \rangle = (s - D)/c$, is (Eqn. B19):

$$\langle t_{\text{del}} \rangle \simeq \left(\frac{\ell_{\text{coh}}}{9c} \right) \left(\frac{D}{r_g(E)} \right)^2 \quad (23)$$

which is

$$\langle t_{\text{del}} \rangle \simeq 3.1 \times 10^5 \left(\frac{ZB_{-9}}{E_{20}} \right)^2 D_2^2 \ell_0 \text{ yr}. \quad (24)$$

We again assume a constant particle energy. All these relations are derived with the implicit assumption that all deviation angles remain small, i.e. $\mathcal{D}_0 s \ll 1$.

The deflection angle α_{rms} and the arrival delay $\langle t_{\text{del}} \rangle$ should be interpreted with some care. Particles originating from the same source will only see statistically independent realisations of the random magnetic field if they diffuse more than one coherence length apart in the direction perpendicular to the unperturbed orbit. The typical perpendicular distance from the original direction of flight at a path length s from the source equals

$$d_{\perp} \equiv \sqrt{\langle x^2 \rangle + \langle y^2 \rangle} = \sqrt{\frac{4}{3} \mathcal{D}_0 s^3}, \quad (25)$$

where we use Eqn. (B17). The requirement $d_{\perp} > \ell_{\text{coh}}$ determines the (energy dependent) *decorrelation distance*:

$$D_{\text{dc}} \simeq \left(\frac{3\ell_{\text{coh}}^2}{4\mathcal{D}_0} \right)^{1/3} = \left(\frac{3}{2} \right)^{2/3} \ell_{\text{coh}}^{1/3} r_g^{2/3}(E), \quad (26)$$

which is

$$D_{\text{dc}} \simeq 30 \ell_0^{1/3} \left(\frac{E_{20}}{ZB_{-9}} \right)^{2/3} \text{ Mpc}. \quad (27)$$

Total decorrelation occurs for $D \gg D_{\text{dc}}$ only. Particles with energies such that the source distance is less than D_{dc} will incur a deviation angle of order α_{rms} , and an arrival delay with a typical magnitude $\langle t_{\text{del}} \rangle$, but the dispersion in these quantities associated with a collection of particles from the same source is expected to be smaller than for particles originating at distances much larger than D_{dc} , which have traversed different magnetic cells. This means that the simulation results of Section 4 should be interpreted differently for $D \lesssim D_{\text{dc}}$ and $D \gg D_{\text{dc}}$. In the first case, the distributions are probability distributions for the time delay, deviation angle etc. averaged over an ensemble of sources. In the second case, particles from a single source will be actually distributed according to the distributions shown. Given the low fluxes above $10^{18.5} \text{ eV}$, it is presently not possible to measure the resulting dispersion from a single source, and only individual arrival directions are measured.

2.3 Spatial diffusion

A description of UHECR propagation in terms of *spatial* diffusion only applies for low energies and/or for large distances.

At low energies, where $r_g(E) \lesssim \ell_{\text{coh}}$, the deflection angle in traversing a *single* cell is already large,

$$\delta\alpha \simeq \frac{\ell_{\text{coh}}}{r_g(E)} \equiv \frac{E_*}{E}, \quad (28)$$

with E_* the characteristic energy for a given field strength and field reversal scale:

$$E_* \equiv ZeB_r \ell_{\text{coh}} \simeq 9.2 \times 10^{17} ZB_{-9} \ell_0 \text{ eV}. \quad (29)$$

Such particles will diffuse through the network of magnetic cells, and presumably within cells if the magnetic turbulence has a broad band spectrum. To describe their propagation, the details of the spectrum of magnetic fluctuations becomes important. As a rough estimate, we assume *Bohm diffusion* with a mean-free-path $\sim r_g(E) = \ell_{\text{coh}} (E/E_*)$ and spatial diffusion coefficient $\mathcal{K}_B \equiv cr_g(E)/3$. In that case the finite age of the Universe, $t \sim H_0^{-1}$, limits the maximum distance of sources contributing to the present-day flux at $E \lesssim E_*$ to

$$\begin{aligned} D_{\text{diff}}(E < E_*) &\sim \left(\frac{c\ell_{\text{coh}}}{H_0} \right)^{1/2} \left(\frac{E}{E_*} \right)^{1/2} \\ &\simeq 55 \ell_0^{1/2} h^{-1/2} \left(\frac{E}{E_*} \right)^{1/2} \text{ Mpc}, \end{aligned}$$

where $h = H_0/(100 \text{ km s}^{-1} \text{ Mpc}^{-1})$.

This essentially means that the Universe is not transparent for cosmic rays with $E < E_*$ *provided* it is filled uniformly with magnetic cells. This estimate ignores the effects of cosmological evolution. These effects are however included the simulations presented in Section 4.

Assuming that UHECRs are indeed of extragalactic origin, this implies an exponential cut-off in the UHECR flux at Earth below $E \simeq E_*$. For particles with $E > E_*$ the deviation angle accumulated by traversing many cells becomes large (see Eqn. B22/23) at a distance of order

$$\lambda(E) = \frac{1}{2\mathcal{D}_0} = \frac{3r_g^2(E)}{2\ell_{\text{coh}}}, \quad (30)$$

which is

$$\lambda(E) = 15 \left(\frac{E_{20}}{ZB_{-9}} \right)^2 \ell_0^{-1} \text{ Gpc} \quad (31)$$

As shown in Appendix B, the propagation of UHECRs on these scales can be treated as spatial diffusion with a diffusion coefficient equal to (Eqn. B25)

$$\mathcal{K} \equiv \frac{D^2}{2t} = c\lambda(E). \quad (32)$$

The finite age of the universe, $t \sim H_0^{-1}$, gives a maximum distance of UHECR sources contributing to the present-day flux:

$$D_{\text{diff}}(E) \simeq \sqrt{\frac{2\mathcal{K}}{H_0}} = \left(\frac{3c\ell_{\text{coh}}}{H_0} \right)^{1/2} \left(\frac{E}{E_*} \right). \quad (33)$$

The rapid energy losses due to photo-pion production above $10^{19.5}/(1+z) \text{ eV}$, followed by a much slower loss at lower energies, means that effectively one can put $E \leq 10^{19.5} \text{ eV}$

in these estimates. So for $E > E_*$, sources contributing to the UHECR flux must be closer than

$$D_{\text{diff}}(10^{19.5} \text{ eV}) \simeq 600 \ell_0^{-1/2} h^{-1/2} (ZB_{-9})^{-1} \text{ Mpc}. \quad (34)$$

2.4 Effects of large-scale structure

So far, we have treated the effects of the intergalactic magnetic field in a simple model where the field consists of randomly oriented cells which are distributed more-or-less homogeneously. Although true observational evidence is lacking, one might argue that magnetic fields follow the distribution of luminous matter and are concentrated mainly in the filamentary large-scale structure of the universe (e.g. de Lapparent et al., 1986). A concentration of strong magnetic fields in the filaments observed in the large-scale structure could be expected, in particular if fields are amplified considerably in the turbulence associated with the formation of galaxies, as proposed by Kulsrud et al. (1997). Such structure in the field distribution is important for the delay incurred by secondary photons produced by the decay of photo-produced neutral pions (Waxman & Coppi, 1996): in the impulsive scenario, the delay of secondary photons will mirror the delay incurred by the UHECRs at their production site with respect to the primary photons associated with the explosive event.

If the IGM magnetic field distribution is strongly structured on scales of $\gtrsim 10 \text{ Mpc}$, the observational upper limit for the typical field strength, $B_r \leq 10^{-9} \text{ G}$, does not apply. Random fields on Mpc scales, concentrated in cluster or superclusters, could be as strong as $10^{-7} - 10^{-6} \text{ G}$. In that case, a totally different model of UHECR propagation should be considered, where particles at lower energy are trapped within clusters in a manner reminiscent of the ‘Leaky Box’ models often used in the description of the propagation and confinement of Galactic cosmic rays (Rachen, 1998 *private communication*). Such a description would extend to particles with energy $E \lesssim 10^{20} Z (B_r/0.1 \mu\text{G}) (L/\text{Mpc}) \text{ eV}$, where L is the size of the cluster.

3 UHECR ENERGY LOSSES

UHECRs with energies above $10^{18.5} \text{ eV}$ lose energy primarily through reactions with photons of the cosmic microwave background (e.g. Berezhinskii et al., 1990 and references therein). Because of the strong energy dependence of scattering on IGM magnetic fields, $\mathcal{D}_0 \propto E^{-2}$, this energy evolution has to be considered in detail when describing the intergalactic propagation of UHECRs. We parameterise the mean energy loss per unit path length by the energy loss length $\ell(E)$ defined by

$$\ell(E) = \left| \frac{1}{E} \frac{dE}{ds} \right|^{-1}. \quad (35)$$

At the lowest energies under consideration in the simulations we will describe in the next Section, $10^{17} \leq E \leq 10^{18} \text{ eV}$, the dominant loss mechanism is (adiabatic) expansion losses in the Hubble flow. The loss length equals the Hubble length,

$$\ell_H \simeq \frac{c}{H_0} \simeq 3 h^{-1} \text{ Gpc}. \quad (36)$$

For protons in the energy range $10^{18.5} < E < 10^{19.5}$ eV, the dominant loss mechanism is photon pair production: $p + \gamma \rightarrow p + e^+ + e^-$ (Blumenthal, 1970). The energy loss length $\ell_p(E)$ for this process reaches its minimum value in the energy range $10^{18.5} < E < 10^{19.5}$ eV (see the figure below and also fig. 3 of Yoshida & Teshima, 1993):

$$\ell_p(E) \simeq 2 \text{ Gpc} . \quad (37)$$

At higher energies, losses are dominated by photo-pion production: $p + \gamma \rightarrow p + \pi$'s. As more and more CMWB photons in the Wien tail of the blackbody spectrum satisfy the threshold condition for pion production at increasing proton energies, the associated loss length $\ell_\pi(E)$ decreases exponentially with increasing energy. In the energy range $10^{19.5} < E < 10^{20.5}$ eV it scales as (see the discussion below)

$$\ell_\pi(E) \simeq 4.8 \left(\frac{E}{E_{\text{th}}} \right)^2 e^{E_{\text{th}}/E} \text{ Mpc} , \quad (38)$$

where $E_{\text{th}} \simeq (m_\pi m_p c^4)/(2k_b T_{\text{CMWB}}) \simeq 3 \times 10^{20}$ eV is the threshold energy. For $E \geq 10^{20.5}$ eV pion production on the CMWB saturates at a constant loss length, as essentially all CMWB photons exceed the threshold in the proton rest frame:

$$\ell_\pi(E) \simeq 10 \text{ Mpc} . \quad (39)$$

The energy loss length in the local universe ($z = 0$) resulting from these combined processes is shown in Figure 1.

In order to describe the UHECR spectrum received at Earth, one has to calculate the modification of the spectrum at the source due to pion-production on the CMWB. A number of pioneering studies have been done in the past (e.g. Berezhinskii, Grigor'eva & Zatsepin, 1975; Hill & Schramm, 1985; Berezhinskii & Grigor'eva, 1988; Rachen & Biermann, 1993; Yoshida & Teshima, 1994 and Aharonian & Cronin, 1994).

Much of the discussion has focussed on the approximation to be used to describe the spectrum near the Greisen-Zatsepin-Kuz'min (GZK) cut-off in the spectrum (Greisen, 1966; Zatsepin & Kuz'min, 1966), which results from the exponential dependence of the photo-pion production loss length (Eqn. 38). This cut-off occurs at an energy $E_c \sim 10^{19.5}$ eV. Particles injected above the cut-off are expected to 'pile up' close to E_c , forming a bump in the spectrum. The height and width of this bump is determined by the details of the pion production process.

Early work (e.g. Berezhinskii & Grigor'eva, 1988) assumed that the effect of pion losses could be described by a simple continuous energy loss approximation, i.e. $dE/ds = -E/\ell(E)$. It was pointed out by Hill & Schramm (1985) that there is an intrinsic spread in energy which is not described by this simple approximation. This spread results from two effects:

- (i) The kinematics of the photo-pion production, which leads to a spread in the energy of particles in the observer's frame due to the spread of pion production angles in the center-of-momentum frame (CMF).
- (ii) The Poisson noise in the number of photons encountered for a given path length s .

These effects modify the result of the continuous loss approximation, spreading the bump over a larger energy range

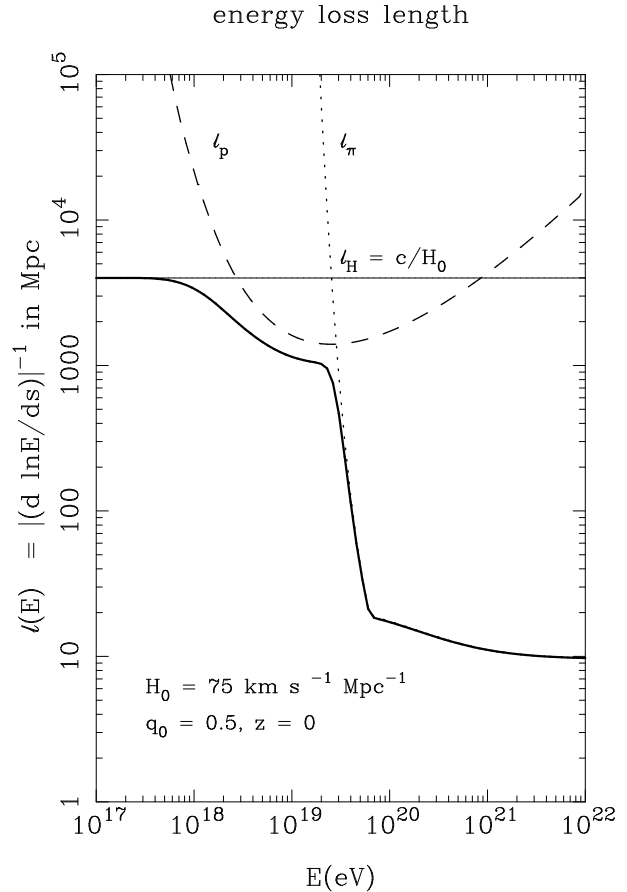


Figure 1. The loss length $\ell(E)$ (thick solid curve) as a function of energy. It is the result of losses due to pion production (ℓ_π , dotted curve), pair losses (ℓ_p , dashed curve) and expansion losses in the Hubble flow ($\ell_H = c/H_0$, horizontal solid line) in a flat Universe ($q_0 = \frac{1}{2}$).

and making it less prominent. In the next section, we will consider a simple model for the evolution of the UHECR spectrum in transit from source to observer due to these effects.

3.1 Kinematics of photo-pion production

Because of its importance in determining the GZK cut-off energy, and the 'survival probability' of UHECRs above the cut-off, we consider photo-pion production in somewhat more detail. A more complete account can be found in Berezhinskii et al. (1975) or in Mannheim & Biermann (1989). All expressions are for protons ($Z = A = 1$), but can be readily generalised to other nuclei. We use units with $c = 1$ in this Section.

The interaction between a proton with energy E_p and a photon with energy ϵ in the observer's frame is most conveniently described in terms of the invariant total energy \overline{E}_t in the center of momentum frame (CMF), which moves with Lorentz factor $\gamma_{\text{CMF}} = (E_p + \epsilon)/\overline{E}_t \simeq E_p/\overline{E}_t \gg 1$, and the photon energy ϵ_0 in the proton rest frame (PRF). They are related by

$$\overline{E}_t = \sqrt{m_p^2 + 2m_p\epsilon_0} , \quad \epsilon_0 = \gamma_p \epsilon (1 - \beta_p \cos \theta) . \quad (40)$$

Here $\gamma_p = 1/\sqrt{1 - \beta_p^2}$ is the Lorentz factor of the proton, and θ the angle between the photon propagation direction and the proton momentum in the lab frame. A head-on collision between proton and photon corresponds to $\theta = \pi$.

Energy and momentum conservation in the CMF, followed by a Lorentz transformation back to the observers frame, yield the following expression for the final proton energy:

$$E_p^f \simeq E_p [1 - K_p + \tilde{K} \cos \sigma_{if}] . \quad (41)$$

Here σ_{if} is the angle between the momentum vector of the incoming and final proton in the CMF. We have put $\beta_{\text{CMF}} \approx 1$, which is an excellent approximation at these energies, and defined a *mean elasticity*

$$K_p \equiv \frac{\bar{E}_t^2 + m_\pi^2 - m_p^2}{2\bar{E}_t^2} . \quad (42)$$

The quantity \tilde{K} is a measure of the spread of final energies around the mean,

$$\tilde{K} \equiv \frac{\sqrt{(\bar{E}_t^2 - m_+^2)(\bar{E}_t^2 - m_-^2)}}{2\bar{E}_t^2} , \quad (43)$$

with $m_\pm \equiv m_p \pm m_\pi$. If one assumes that the CMF production angle σ_{if} is distributed isotropically, the *mean* energy loss per interaction in the observer's frame equals $\Delta E_p = -K_p E_p$ and the energy dispersion is $\Delta E_{\text{rms}} \simeq (\tilde{K}/\sqrt{3}) E_p$.

The spread in the final proton energy in the observer's frame increases strongly with CMF energy. Near reaction threshold, which corresponds to zero momentum for the final proton and the production of a single pion at rest so that $\bar{E}_t \simeq m_p + m_\pi$, one has $K_p \simeq 0.13$ and $\tilde{K} \approx 0$, and the spread in the final proton energies in the observer's frame is small. Much above threshold, where $\bar{E}_t \gg m_+$ and $K_p \approx \tilde{K} \approx \frac{1}{2}$, one has $E_p^f \approx \frac{1}{2} E_p (1 + \cos \sigma_{if})$, so the spread in final energies is large.

The interaction rate for photo-pion production in the observer's frame, $\mathcal{R}_{p\gamma}$, can be expressed in terms of the reaction cross-section $\sigma_0^{p\gamma}(\epsilon_0)$ in the PRF by using the Lorentz-invariance of the photon occupation number in phase space and the relativistic aberration formulas which, in the limit $\gamma_p \gg 1$, lead to strong relativistic beaming of the CMWB photons in the PRF, so that all photons have $\cos \theta_0 \simeq -1$. The relevant expressions can be found in Blumenthal (1970).

This leads to an expression for the reaction rate derived by Berezhinskii *et al.* (1975), but with corrected integration limits corresponding to the kinematically allowed values:

$$\mathcal{R}_{p\gamma} = \int_{\epsilon_{\text{th}}/2\gamma_p}^{\infty} d\epsilon \frac{n(\epsilon)}{\epsilon^2} \left(\frac{1}{2\gamma_p^2} \int_{\epsilon_{\text{th}}}^{2\gamma_p \epsilon} d\epsilon_0 \sigma_0^{p\gamma}(\epsilon_0) \epsilon_0 \right) . \quad (44)$$

Here $\epsilon_{\text{th}} = m_\pi(1 + m_\pi/2m_p) \simeq 145$ MeV is the photon threshold energy in the PRF. Berezhinskii *et al.* (1975) incorrectly replace the upper limit on the integration over ϵ_0 for fixed ϵ by infinity. For a thermal (Planckian) photon distribution in the observer's frame with temperature T one has, reinstating c :

$$\frac{n(\epsilon)}{\epsilon^2} = \frac{1}{\pi^2(\hbar c)^3} [e^{\epsilon/k_b T} - 1]^{-1} . \quad (45)$$

The PRF pion production cross-section $\sigma_0^{p\gamma}(\epsilon_0)$ near threshold is dominated by a resonance in the $p + \gamma \rightarrow p + \pi^0$

reaction near $s = \bar{E}_t^2 \simeq 1.6 \text{ GeV}^2 \equiv s_m$ with $\sigma^{p\gamma}(s_m) \simeq 0.5$ mb. Therefore, not too far from threshold, we can approximate the cross-section by

$$\sigma^{p\gamma}(s) \simeq \Delta s \sigma^{p\gamma}(s_m) \delta(s - s_m) \quad (46)$$

in the integral over ϵ_0 or s . Here $\Delta s \simeq m_p \epsilon_{\text{th}} \simeq 0.15 \text{ GeV}^2$ is the width of the resonance. The value of s_m corresponds to $\epsilon_0 \simeq 0.3 \text{ GeV} \approx 2\epsilon_{\text{th}}$.

Using the above approximation for the cross-section, the reaction rate for $E_p \ll E_{\text{th}}$ typically equals

$$\mathcal{R}_{p\gamma}(E_p) \simeq \frac{4}{\pi^2} \left(\frac{k_b T}{\hbar c} \right)^3 c \sigma_m \left(\frac{E_{\text{th}}}{E_p} \right)^2 e^{-E_{\text{th}}/E_p} , \quad (47)$$

with $\sigma_m = \sigma^{p\gamma}(s_m)$, and $E_{\text{th}} = (m_\pi m_p c^4)/(2k_b T)$. Putting $E_{\text{th}}^2 = s_m$ in Eqns. (42) and (43) yields $K_p \simeq 0.2$ and $\tilde{K} \simeq 0.165$ in this limit.

At energies $E_p \gg E_{\text{th}}$, $\bar{E}_t \gg m_p + m_\pi$, the cross-section summed over all reactions becomes approximately constant, $\sigma^{p\gamma}(s) \simeq 0.16 \text{ mb} \equiv \sigma_0$. The reaction rate $\mathcal{R}_{p\gamma}(E_p)$ then approaches the constant rate

$$\mathcal{R}_{p\gamma}(E_p \gg E_{\text{th}}) \simeq 0.244 \left(\frac{k_b T}{\hbar c} \right)^3 c \sigma_0 , \quad (48)$$

while the mean fractional energy change and energy dispersion satisfy $K_p \simeq \tilde{K} \simeq 0.5$. The energy loss length $\ell(E)$ follows from these quantities as

$$\ell(E) = c / (\mathcal{R}_{p\gamma}(E) K_p) . \quad (49)$$

3.2 Effects of Poisson noise

The *mean* number of pion-producing photons encountered by UHECR particles in a path length $\Delta s = c\Delta t$ equals

$$\langle n_{\text{ph}} \rangle (\Delta s) \simeq \frac{\mathcal{R}_{p\gamma} \Delta s}{c} = \frac{\Delta s}{K_p \ell(E)} . \quad (50)$$

The *actual* number of photons encountered by an individual particle is subject to Poisson statistics. This means that the variance in the number of encounters equals $\chi_n = \langle n_{\text{ph}} \rangle^{1/2}$, while the probability of a particle not encountering *any* photons decays as $P(n_{\text{ph}} = 0) = e^{-\langle n_{\text{ph}} \rangle}$. The effect of Poisson statistics is especially important for protons at high energies, $E_p \geq 10^{18.5} \text{ eV}$, where $K_p \ell(E) \simeq 20 \text{ Mpc}$. For protons originating from sources closer than $D \sim 20 - 50 \text{ Mpc}$, the effect of Poisson statistics on the energy loss should be clearly visible in the arrival spectrum. There is a significant fraction of particles which have interacted with no (or only a few) photons, leading to a high-energy tail in the spectrum which more or less reflects the original source spectrum, because the loss length $\ell(E)$ is roughly independent of energy, but at an amplitude reduced by a factor $\sim e^{-\langle n_{\text{ph}} \rangle(D)}$.

4 SIMULATIONS

We have constructed a simulation code for the propagation of protons in intergalactic space, taking into account the scattering on IGM magnetic fields and the energy losses suffered as a result of interactions with the CMWB.

The propagation of the UHECRs over a path length Δs is calculated with the simple explicit scheme

$$\mathbf{x}(s + \Delta s) = \mathbf{x}(s) + \hat{\mathbf{n}}(s) \Delta s. \quad (51)$$

The unit vector $\hat{\mathbf{n}}$ along the direction of propagation undergoes diffusion, which is described by the explicit numerical integration of a stochastic differential equation (SDE). The stochastic change in the direction of flight is modelled by

$$\Delta \hat{\mathbf{n}}_{\text{st}} = \sqrt{2\mathcal{D}_0 \Delta s} (\xi_1 \mathbf{e}_1 + \xi_2 \mathbf{e}_2). \quad (52)$$

Here ξ_1 and ξ_2 are two independent unit Wiener processes, drawn at each step from a Gaussian distribution with unit dispersion so that $\langle \xi_{1,2} \rangle = 0$, $\langle \xi_{1,2}^2 \rangle = 1$. The two (arbitrary but mutually orthogonal) unit vectors $\mathbf{e}_{1,2}$ lie in a plane perpendicular to $\hat{\mathbf{n}}$ so that $\Delta \hat{\mathbf{n}}_{\text{st}} \cdot \hat{\mathbf{n}} = 0$. Note that $\hat{\mathbf{n}} \equiv (n_1, n_2, n_3)$ and $\mathbf{e}_{1,2}$ are the eigenvectors (with eigenvalues 0 and 1 respectively) of the diffusion tensor $\mathcal{D}_{ij} = \mathcal{D}_0 P_{ij}$, with $P_{ij} \equiv (\delta_{ij} - n_i n_j)$, which motivates this approach. This prescription is equivalent to the stochastic term in Eqn. (B1) of Appendix B, with the correspondence

$$\sqrt{2\mathcal{D}_0} \mathbf{P}(\hat{\mathbf{n}}) \cdot \Delta \mathbf{W} \longrightarrow \sqrt{2\mathcal{D}_0 \Delta s} (\xi_1 \mathbf{e}_1 + \xi_2 \mathbf{e}_2). \quad (53)$$

The new propagation direction then is calculated as

$$\hat{\mathbf{n}}(s + \Delta s) = \sqrt{1 - |\Delta \hat{\mathbf{n}}_{\text{st}}|^2} \hat{\mathbf{n}}(s) + \Delta \hat{\mathbf{n}}_{\text{st}}. \quad (54)$$

This preserves the norm $\hat{\mathbf{n}} \cdot \hat{\mathbf{n}} = 1$ and is an excellent approximation for the diffusion process provided $|\Delta \hat{\mathbf{n}}_{\text{st}}| \ll 1$. When many independent realizations of these SDEs are simulated, the resulting distribution of unit vectors corresponds to a solution of the diffusion equation for $\hat{\mathbf{n}}$. Details of similar astrophysical applications of SDEs can be found in Achterberg & Krüß (1992).

The change in UHECR energy is calculated as the combined effect of expansion losses in the the Hubble flow, pair production and photo-pion production losses. Pair production is treated using the continuous loss approximation, $(dE/ds)_p = -E/\ell_p$, which is an excellent approximation for this process. We use the interpolation formula of Stepney & Guilbert (1983) for the cross-section as a function of proton energy, and the numerical fit of Chodorowski, Zdziarski & Sikora (1992) for the inelasticity of the reaction. The integration over the CMWB photon distribution in the proton rest frame proceeds along the lines elaborated in Section 3. The pair production loss length $\ell_p(E)$ so obtained (see Figure 1) closely follows the result of Blumenthal (1970).

Pion production must be treated in more detail. The number of pion-producing photons encountered in a path-length increment Δs is drawn from a Poisson distribution with mean $\langle n_{\text{ph}} \rangle = \Delta s / \ell_{p\gamma}$. The interaction length $\ell_{p\gamma} \equiv c/\mathcal{R}_{p\gamma}$ is calculated according to (with threshold energy $E_{\text{th}} \sim 3 \times 10^{20}$ eV):

$$\ell_{p\gamma}(\text{Mpc}) = \begin{cases} 0.9 \left(\frac{E}{E_{\text{th}}} \right)^2 e^{E_{\text{th}}/E} & (E \leq 0.2 E_{\text{th}}), \\ 4.8 & (E > 0.2 E_{\text{th}}). \end{cases} \quad (55)$$

Here we have written E rather than E_p for the proton energy. The energy loss per interaction is calculated using a simple interpolation formula for the mean inelasticity:

$$K_p = 0.2 \left(\frac{E_{\text{th}} + 2.5E}{E_{\text{th}} + E} \right). \quad (56)$$

inelasticity

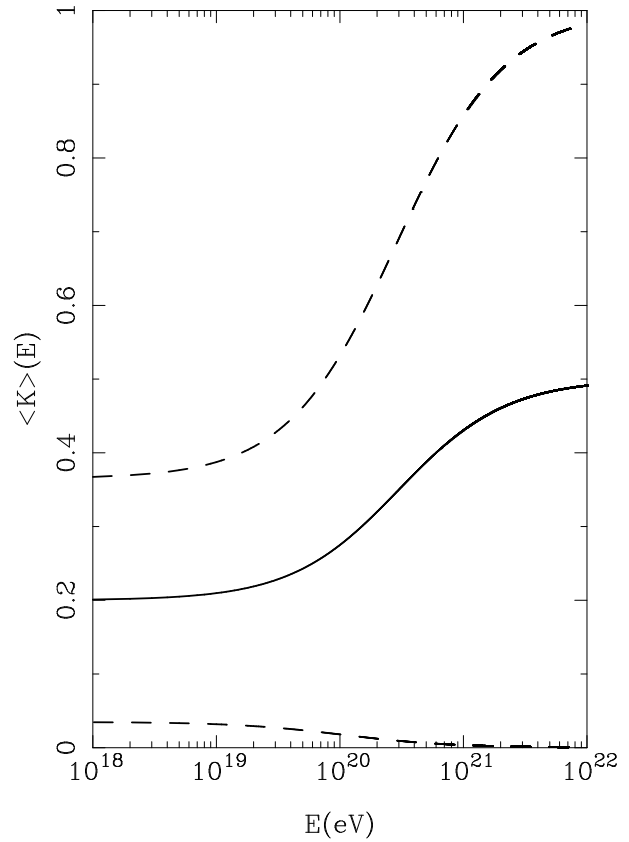


Figure 2. The mean inelasticity $\langle K \rangle \equiv K_p$ (solid line) and the upper and lower limit (dashed lines), corresponding to $\langle K \rangle \pm \tilde{K}$, due to the variance in production angle σ_{if} in the PRF. At given energy, the inelasticity is uniformly distributed between the dashed lines.

The pion production angle in the center of momentum frame is drawn from a uniform distribution $-1 \leq \cos \sigma_{\text{if}} \leq 1$. The energy change is calculated according to Eqn. (41), with \tilde{K} calculated by re-expressing \bar{E}_t^2 in terms of K_p using the exact kinematic relations for K_p and \tilde{K} :

$$\tilde{K} \equiv \sqrt{(K_p + K_+)(K_p - K_-)}, \quad (57)$$

with $K_{\pm} \equiv m_{\pi}/(m_p \mp m_{\pi})$. This allows the use of a single interpolation for $K_p(E)$ while preserving the correct behaviour of \tilde{K} at both low and high energies. This is illustrated in Figure 2.

Finally, at large source distances cosmological effects are taken into account. Due to the higher CMWB photon density and temperature at a distance corresponding to a redshift z , $n_{\text{ph}} \propto (1+z)^3$ and $T_{\text{CMWB}} \propto (1+z)$, the energy loss length due to interaction with CMBW photons at redshift z can be obtained from the value in the local universe ($z = 0$) by using the scaling law

$$\ell(E, z) = \frac{\ell((1+z)E, z=0)}{(1+z)^3}. \quad (58)$$

This is a simple consequence of the fact that the loss length is inversely proportional to the photon number density and depends on energy E and the lab frame threshold energy

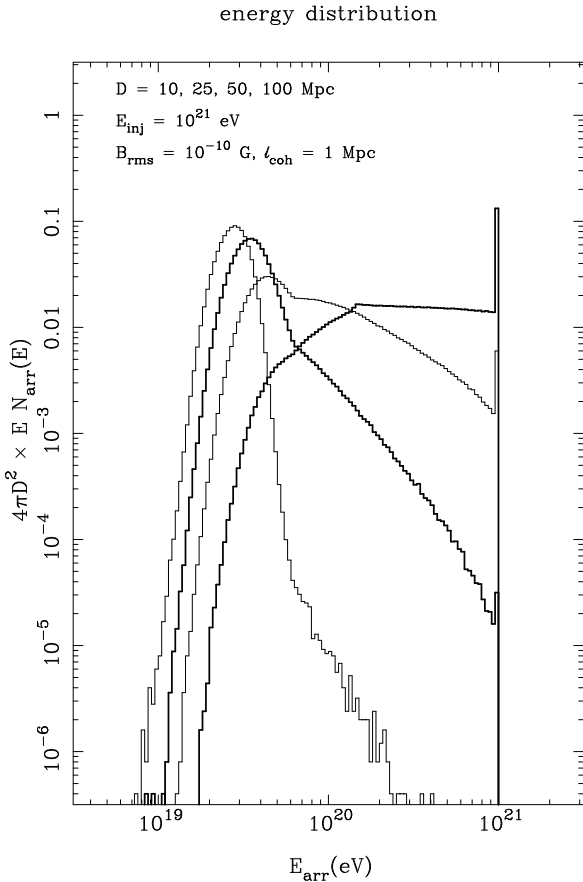


Figure 3. Arrival spectra at Earth for mono-energetic injection at an energy of 10^{21} eV at the source, for four source distances D . The spectra have been multiplied by an arbitrary factor $\propto D^2$. For increasing distance, the maximum of the spectrum shifts to lower energy. For 10 Mpc there is still a significant fraction of particles at the injection energy, giving rise to a distinct spike. This spike has almost completely vanished for $D = 50$ Mpc. The spectrum above $10^{19.5}$ eV, where the loss length $\ell(E)$ decreases by almost two orders of magnitude, decreases rapidly for larger distances.

$E_{\text{th}} \propto T_{\text{CMBW}}^{-1} \propto (1+z)^{-1}$ of the interaction through the ratio $E/E_{\text{th}} \propto 1+z$.

The random magnetic field strength in the general intergalactic medium scales as $B_r \propto (1+z)^2$ as a result of flux freezing in an expanding universe (e.g. Subramanian & Barrow, 1998). The universal expansion stretches the correlation length so that $\ell_{\text{coh}}(z) = \ell_{\text{coh}}(z=0)/(1+z)$. As a result of these effects the magnitude of the flight direction diffusion rate scales as $D_0 \propto B_r^2 \ell_{\text{coh}} \propto (1+z)^3$. In our simulations we assume a flat, matter-dominated universe in which the Hubble length scales as $\ell_H = (c/H_0) \times (1+z)^{-3/2}$.

4.1 Simulation results

To illustrate the effects of UHECR scattering most clearly, we consider the case of mono-energetic injection first. Particles are injected with an energy $E_{\text{inj}} = 10^{21}$ eV. Arrival spectra, delay times and angular distributions are calculated for different source distances. Figure 3 shows the arrival spectra.

From this calculation it is obvious that the effect of

Poisson statistics remains strong up to distances of about 50 Mpc: a tail of high-energy particles up to the injection energy remains. At larger distances, the probability of not encountering any CMBW photons becomes vanishingly small. Energy losses proceed much more slowly once particles reach an energy $E < 10^{19.5}$ eV, as the loss length becomes larger than 1 Gpc. Therefore particles tend to accumulate around $10^{19.5}$ eV, drifting slowly to lower energies.

Figure 4 shows the distribution of the delay time with respect to simultaneously produced photons, for a number of different source distances. At small distances they are centered around a value close to the predicted value of t_{del} for the injection energy of 10^{21} eV. For those distances larger than 25 Mpc, the delay distribution has its maximum close to the value of t_{del} associated with the typical arrival energy, $E_{\text{arr}} \approx 10^{19.5}$ eV.

Figure 5 shows the cumulative angular distribution of the UHECRs for the arrival angle α' with respect to the line of sight to the source. The deflection process considered here will lead for constant particle energy to an angular distribution of the form $dN/d\Omega \propto \exp(-\alpha'^2/\alpha_{\text{rms}}^2)$, with $d\Omega = 2\pi \sin \alpha' d\alpha'$. For small angles, α' and $\alpha_{\text{rms}} \ll 1$, this distribution scales as

$$\frac{dN}{d \ln \alpha'} \propto \alpha'^2 e^{-\alpha'^2/\alpha_{\text{rms}}^2}, \quad (59)$$

which has a maximum at $\alpha' = \alpha_{\text{rms}}$. The simulated distributions shown in Figure 5, calculated with energy losses taken into account, closely resemble model distribution (59).

Next we consider the case of power-law injection, where particles are produced at the source according to

$$dN_{\text{inj}}(E) = n_{\text{inj}}(E) dE = \kappa E^{-s} dE. \quad (60)$$

Figure 6 shows the arrival spectrum at Earth as expected for a steady source. The injection spectrum was $n(E) \propto E^{-2}$ between 10^{17} and 10^{21} eV. The delay incurred in transit has a negligible influence on the shape of the spectrum as long as $ct_{\text{del}} \ll D$. Therefore the arrival spectra calculated for $B_{\text{rms}} = 10^{-11}$ G and $\ell_{\text{coh}} = 1$ Mpc are representative for all simulations we performed at energies well above $E_* \approx 10^{18} Z B_{-9} \ell_0$ eV. The spectra have been multiplied with a factor $\propto D^2 E^2$ so that the injection spectrum in all cases corresponds to a horizontal line. For energies below 10^{19} eV, the effect of losses is negligible at these source distances. Particles do accumulate at the GZK cut-off energy, but the height of the ‘bump’ is not very dramatic due to the natural spread in arrival energies, $\Delta E/E \simeq \mathcal{O}(1)$ for a given injection energy due to the variance in the photo-pion production kinematics. The high-energy tail above the GZK cut-off is very pronounced at $D = 10$ and at $D = 25$ Mpc, still quite visible in the 50 Mpc curve, but almost absent at a source distance $D = 100$ Mpc. Our results are qualitatively similar to those obtained by Yoshida & Teshima (1993) in the corresponding distance range.

Figure 7 shows the delay time t_{del} and the dispersion Δt_{del} (shown with error bars as $t_{\text{del}} \pm \Delta t_{\text{del}}$) for particles originating at $D = 25$ Mpc as a function of the arrival energy E_{arr} at Earth. The delay time has been scaled by a factor $\propto (E_{\text{arr}}/10^{20} \text{ eV})^2$ to scale away the dominant energy dependence predicted by Eqn. (23). Particles well below the GZK cut-off ($E < 10^{19}$ eV) have lost little energy, and there-

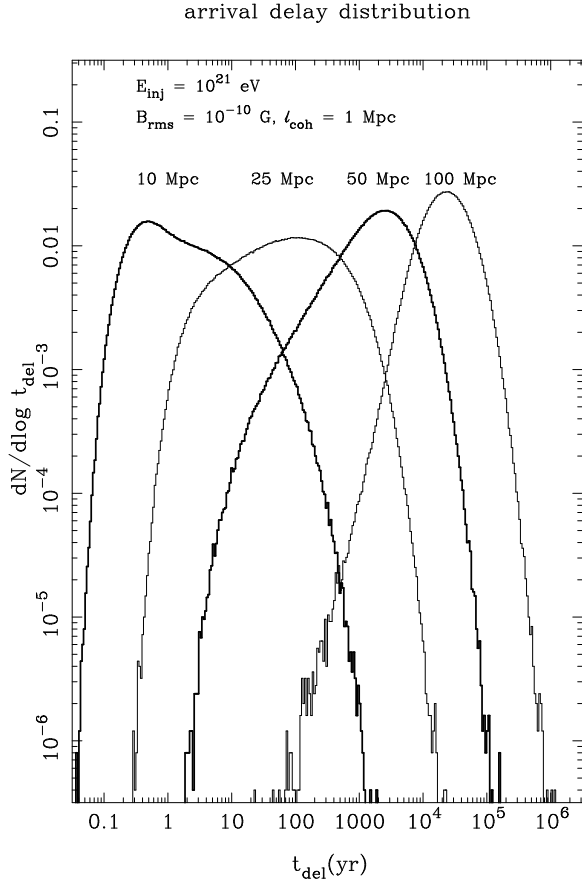


Figure 4. Delay time distribution at Earth for particles mono-energetically injected at $E = 10^{21}$ eV for four source distances ranging from 10 to 100 Mpc. The distribution for the smallest distance is the left-most curve, for the largest distance the right-most curve. The maximum in the 10 Mpc curve coincides with the theoretical result of Eqn. 24 for that distance at the injection energy, $t_{\text{del}}(10^{21} \text{ eV}) \simeq 0.3$ year. The maximum for the 100 Mpc curve coincides roughly with the theoretical result for that distance and the energy where most particles reside (see figure 3): $E \sim 2 \times 10^{19}$ eV, yielding $t_{\text{del}} \simeq 10^5$ year

fore fall almost on the horizontal line predicted by Eqn. (24) for $Z = 1$ (protons):

$$t_{\text{del}}(E, D) \ell_0^{-1} (E_{20}/B_{-9}D_2)^2 \simeq 0.31 \text{ Myr} . \quad (61)$$

At the lowest energies considered here, $E \simeq 10^{17}$ eV, there is an increase in the delay time because the small deflection angle approximation starts to break down: $\alpha_{\text{rms}} \simeq 20^\circ$ at these energies. Well above the GZK cut-off the delay time is roughly half the expected value based on the arrival energy due to the fact that the mean energy in transit is larger than the arrival energy. For energies near the injection energy, $E \approx 10^{21.5}$ eV, the delay time once again approaches the theoretical value as these are particles that happen not to have interacted significantly with CMWB photons, and have therefore propagated with an almost constant energy.

Figure 8 shows the dispersion in delay times, σ_{del} , as a function of the delay time for the same arrival energy bins as in Figure 7, with the dominant energy dependence scaled away. From this figure one can conclude that, at least in the

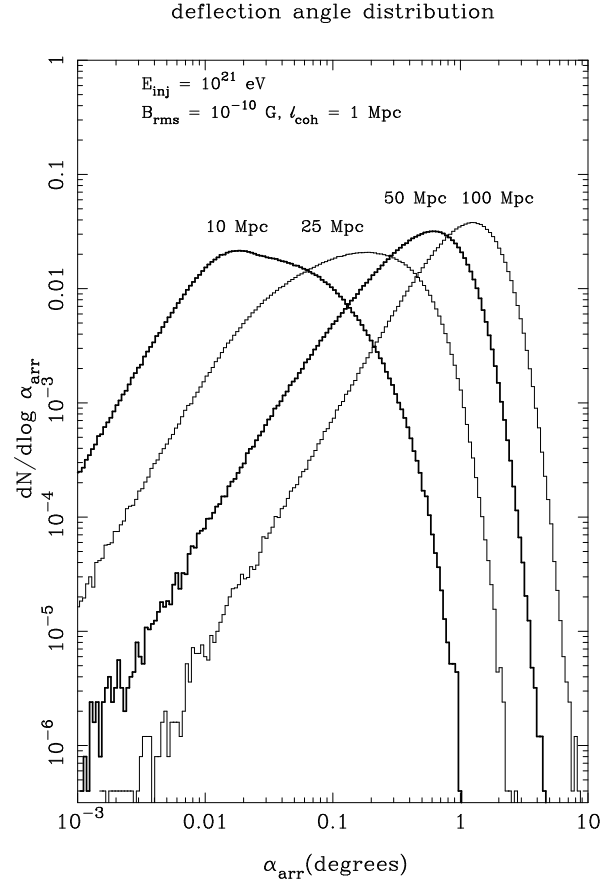


Figure 5. Angular distribution at Earth of the arrival angle $\alpha_{\text{arr}} \equiv \alpha'$ with respect to the line-of-sight to the source, for particles monochromatically injected at $E = 10^{21}$ eV for distances ranging from 10 to 100 Mpc. The maximum of these curves is roughly at α_{rms} (Eqn. 22). For a distance of 10 Mpc and $E \sim 10^{21}$ eV, theory predicts $\alpha_{\text{rms}} \simeq 0.012$ degrees. For a distance of 100 Mpc and an energy of $E \sim 2 \times 10^{19}$ eV, one expects $\alpha_{\text{rms}} \simeq 2$ degrees.

regime considered here, the often-used approximation (e.g. Miralda-Escudé & Waxman, 1996)

$$\sigma_{\text{del}}(E, D) \equiv \sqrt{\langle (t_{\text{del}} - \langle t_{\text{del}} \rangle)^2 \rangle} \simeq t_{\text{del}}(E, D) \quad (62)$$

is a fair one. We find roughly $\sigma_{\text{del}} \approx 0.6 \langle t_{\text{del}} \rangle$, but this relation is approximate, and breaks down when the delays (and deflection angles) become large (not shown).

Figure 9 shows the angle $\alpha' = \cos^{-1}(\hat{n} \cdot \hat{r})$ with respect to the line of sight to the source as a function of arrival energy. The dominant behaviour, $\alpha' \propto E^{-1}$, has been scaled away. If particles did not lose energy, the arrival angle would satisfy (Eqn. 22)

$$\alpha' \times \left(\frac{E_{20}}{B_{-9}} \right) (D_2 \ell_0)^{-1/2} \simeq 3.5^\circ . \quad (63)$$

The actual value (using $E = E_{\text{arr}}$) is somewhat less as a result of the energy losses.

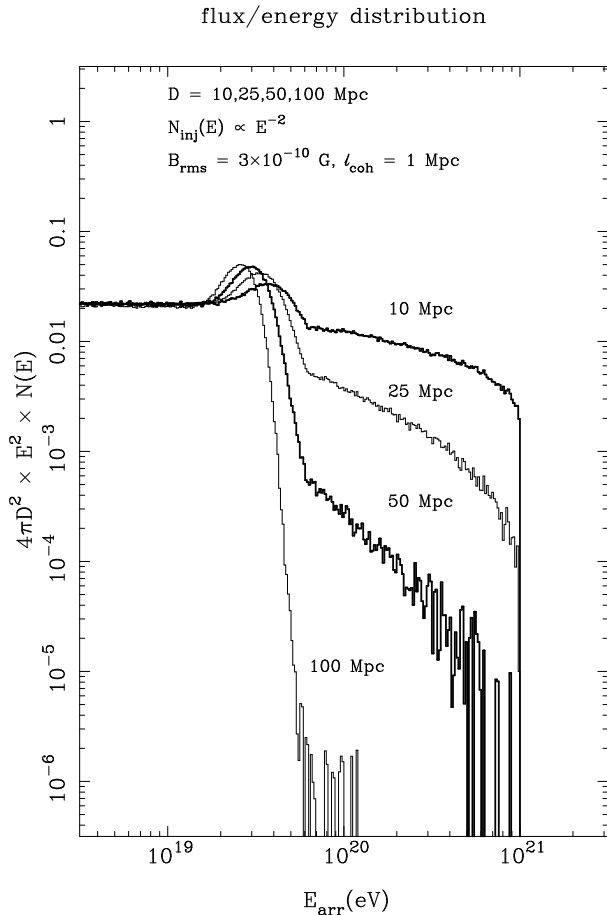


Figure 6. Energy distribution $n(E) \times E^2$, received at Earth for a continuously radiating source. Particles are injected at the source with $n_{\text{inj}}(E) \propto E^{-2}$ between $10^{17} \leq E \leq 10^{21}$ eV. Spectra are calculated for a source distance D equal to 10, 25, 50 and 100 Mpc, and multiplied by an arbitrary factor $\propto D^2$. Only the portion of the spectrum between $10^{18.5}$ and $10^{21.5}$ eV is shown. This figure should be compared with figure 3 for monochromatic injection. There is a clear ‘bump’ near the GZK cut-off at $E \sim 10^{19.5}$ eV. Below the GZK cut-off, particles lose energy very slowly ($\ell(E) \geq 1$ Gpc), and the spectrum is almost independent of source distance.

5 BURSTING SOURCES AND THE GZK CUT-OFF

Observations in the northern hemisphere show the arrival direction of events above 4×10^{19} eV to be distributed over the whole sky, but with some evidence for clustering of arrival directions around the supergalactic plane (Stanev *et al.*, 1995; Hayashida *et al.*, 1996). A similar analysis of the less extensive data set from the southern hemisphere (Kewley *et al.*, 1996) does not show evidence for this clustering.

Due to photo-pion production on the CMWB (Greisen, 1966; Zatsepin & Kuz'min, 1966) it is likely that particles with energy above $10^{19.5}$ eV originate from a volume with radius $D < D_{\text{max}} \simeq 50$ Mpc. Deflection by random intergalactic magnetic fields over a distance $D \leq D_{\text{max}}$ is not capable of deflecting UHECRs in this energy range by more than 5–10 degrees, given the observational limit on the field amplitude B_{rms} .

This means that the observed UHECRs in the energy

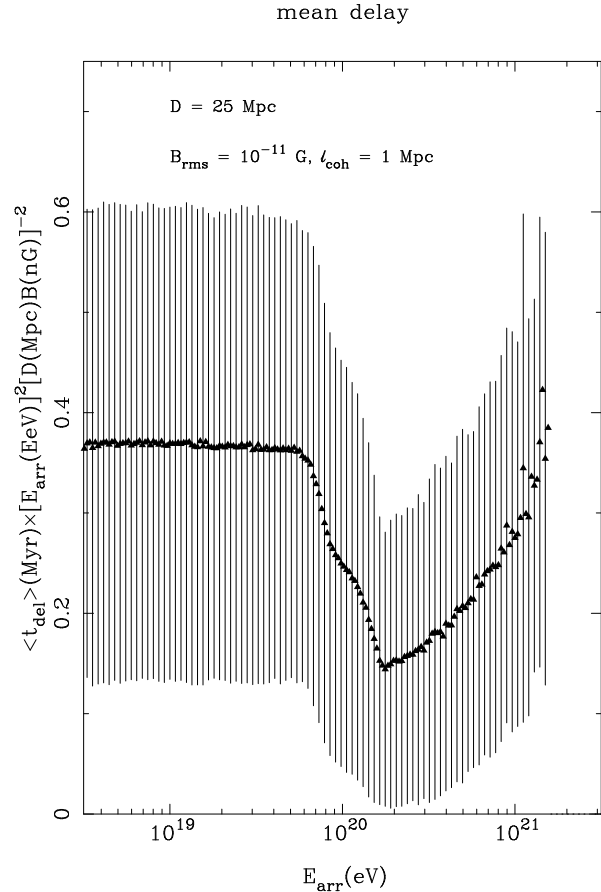


Figure 7. Delay time as a function of arrival energy. The dispersion in the delay time is shown as error bars. The delay has been scaled such that propagation at *constant* energy E would result in a horizontal line at $t_{\text{del}} \times E_{\text{TeV}}^2 / (D_{\text{Mpc}} B_{\text{nG}})^2 \simeq 0.31$ Myr, cf. Eqn. 24. One sees that for the particles near $E_{\text{max}} = 10^{21.5}$ eV, which happen to have lost little energy, and for the particles in the range $E < 10^{19.5}$ eV which, at this source distance, have lost very little energy, this theoretical value is approximated. For $10^{20} \text{ eV} < E < 10^{21}$ eV the influence of energy losses reduces t_{del} with respect to the value predicted on the basis of the arrival energy E_{arr} .

range above $10^{19.5}$ eV (some ~ 100 events, with about 7 events above 10^{20} eV) must originate from multiple sources. Solely on the basis of simple energy arguments (Rachen & Biermann, 1993; Norman, Melrose & Achterberg, 1995), only the most luminous radio galaxies (FRII sources) or shocks associated with ongoing large-scale (\sim Mpc) structure formation can continuously produce particles in this energy range. Production sites in the case of radio galaxies are the so-called *hot spots*, where the impact of large-scale collimated jets on the intergalactic gas creates strong, large (\sim kpc scale) shocks. The typical space density of Fanaroff-Riley II radio galaxies in the local universe is small, $n_s \simeq 10^{-7} \text{ Mpc}^{-3}$. The corresponding distance scale, $D_s = (4\pi n_s/3)^{-1/3} \simeq 100$ Mpc, is large compared with the typical loss length for particles above $10^{19.5}$ eV, $\ell(E) \simeq 10$ Mpc. If there is still ongoing structure formation in the local universe, the sky filling factor of the filamentary shocks associated with this process would be small.

It is therefore not surprising that no clear candidate

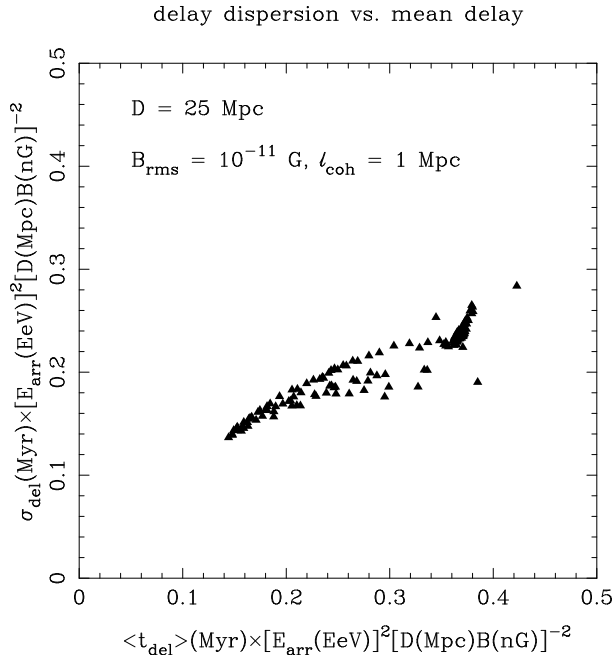


Figure 8. Delay time dispersion σ_{del} as a function of mean delay time $\langle t_{\text{del}} \rangle$ for a source at a distance of 25 Mpc in a 0.01 nG field. The dominant energy dependence $\propto E^{-2}$ has been scaled away. The normalization of the delay time and delay dispersion is as in figure 7. At this distance and field strength, where the small-angle approximation for the deflection process still applies, one can fit the delay dispersion roughly with a linear relation of the form $\sigma_{\text{del}} \sim 0.6 \langle t_{\text{del}} \rangle$.

sources for UHECR events have been identified (Elbert & Sommers, 1995). Even if one broadens the candidate sources to include *all* active galaxies, $n_s \simeq 10^{-5} \text{ Mpc}^{-3}$, $D_s \simeq 20 \text{ Mpc}$, one is hard-pressed to find a sufficient number of candidate sources within the local volume bounded by D_{max} , the total number of sources scaling as

$$N_s(D \leq D_{\text{max}}) = \left[\frac{D_{\text{max}}}{D_s} \right]^3. \quad (64)$$

A consequence of this is that the UHECR spectrum at Earth is always dominated by a few close-by sources in the case of continuous production. This is illustrated in figures 10 and 11. These show two representative cases of the UHECR energy distribution, obtained by a discrete distribution of sources within a distance of $D_{\text{in}} = 250 \text{ Mpc}$, each source distance drawn by Monte Carlo simulation from a distribution satisfying Eqn. (64). The figure also shows a calculation of the background contribution due to sources at distances from 250 Mpc to 2.5 Gpc. This background has been calculated using a continuous approximation for the source density. The source density assumed equals $n_s = 10^{-6} \text{ Mpc}^{-3}$, so that $D_s \simeq 70 \text{ Mpc}$. Particles originating at dis-

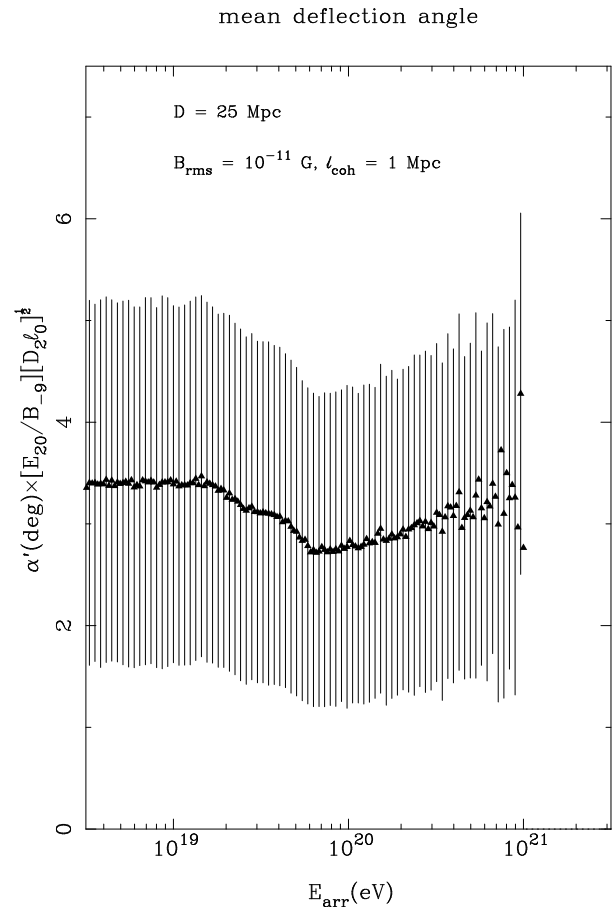


Figure 9. The arrival angle with respect to the line of sight to the source as a function of the arrival energy E_{arr} . The dominant parameter dependence $\propto (B\sqrt{D\ell_{\text{coh}}})/E$ has been scaled away so that particles propagating with constant energy would lie on a horizontal line $\alpha' \times (E_{20}/B_{-9}\sqrt{D_2\ell_0}) = 3.5^\circ$. Particles have been injected with energies uniformly distributed over the range $10^{18} < E < 10^{21} \text{ eV}$ at a distance of 25 Mpc, and propagate through a random field with $B_{\text{rms}} = 10^{-11} \text{ G}$ and $\ell_{\text{coh}} = 1 \text{ Mpc}$. The dispersion in the arrival angle is shown as bars. Particles with $E < 10^{19} \text{ eV}$ which lose very little energy for this source distance follow the theoretical result for constant energy propagation.

tances larger than 2.5 Gpc will not reach Earth within a Hubble time due to the large accumulated delay. These figures show that the high-energy part of the spectrum above the GZK cut-off at $10^{19.5} \text{ eV}$ is almost completely dominated by the single closest source.

This simple argument lends some additional credence to the gamma-ray burster hypothesis of Waxman (1995a), Vietri (1995) and Milgrom & Usov (1995), where UHECRs are produced in bursts.

An important difference with the case where UHECRs are produced continuously is the fact that in this case the number of sources contributing to the UHECR flux at Earth at any given time depends critically on the time delay $t_{\text{del}}(E, D)$ incurred during propagation: each source remains visible for a time $\Delta t \simeq t_{\text{del}}$ as a result of the spread in arrival times. At any one time, one sees those sources that have burst within a time interval $\Delta t \simeq t_{\text{del}}$, so that

$$dN_s \simeq 4\pi D^2 Q_{\text{GRB}} t_{\text{del}}(E, D) dD \quad (65)$$

flux from continuous sources

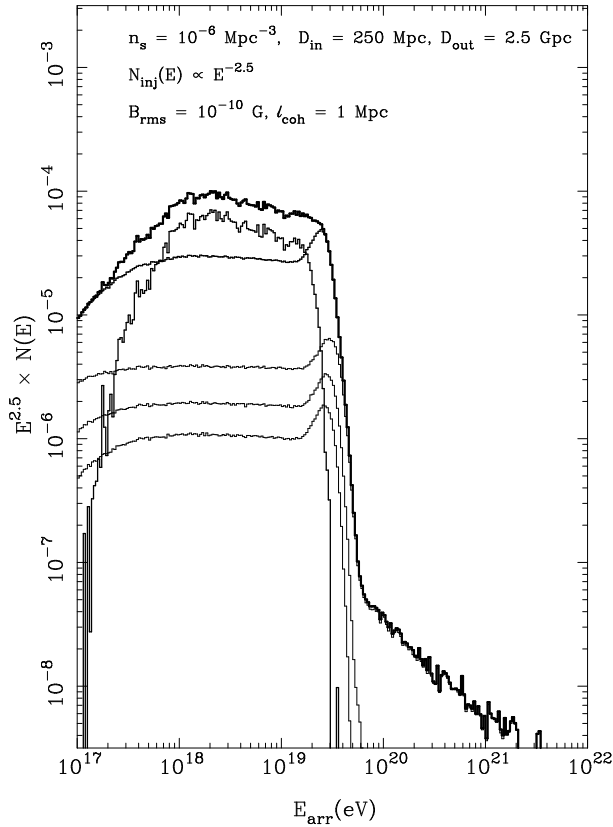


Figure 10. The UHECR spectrum due to continuous sources with a source density of 10^{-6} Mpc^{-3} . It is assumed that all sources are identical in injected flux, and that they are distributed homogeneously in space so that $N(\leq D) \propto D^3$. A Monte-Carlo realization with discrete sources is used for $D < D_{\text{in}} = 250 \text{ Mpc}$. The background of distant sources is calculated using a continuous distribution of source distances between 250 Mpc and 2.5 Gpc for the simulated UHECRs. The injection spectrum is a power-law, $N(E) = \kappa E^{-2.5}$. The dominant power-law behaviour has been scaled away. The thickest line is the total spectrum. The two thinner lines are the contribution of the sources within 250 Mpc and of the background due to more distant sources, which only contributes below the GZK cut-off at $10^{19.5} \text{ eV}$. The three thinnest curves are the spectra of the three closest sources in this realization of the source distribution. It is seen that the closest source completely dominates the spectrum above the GZK cut-off. At energies below $10^{17.5} \text{ eV}$ the closest source again dominates the flux as particles from far-away sources do not reach the observer within a Hubble time due to the slow spatial diffusion of particles in this energy range.

sources contribute to the flux at energy E from a spherical shell of thickness dD at distance D . Here Q_{GRB} is the typical gamma ray burst rate per unit volume in the cosmological scenario. The typical value of Q_{GRB} in a non-evolving scenario, where GRBs are distributed homogeneously within a volume corresponding to a redshift $z \leq 1$, is of order

$$Q_{\text{GRB}}^{\text{hom}} \simeq 10^{-8} \left(\frac{H_0}{75 \text{ km s}^{-1} \text{ Mpc}^{-1}} \right)^{-3} \text{ Mpc}^{-3} \text{ yr}^{-1}. \quad (66)$$

The total energy yield per burst is typically $E_{\text{GRB}} \simeq$

flux from continuous sources

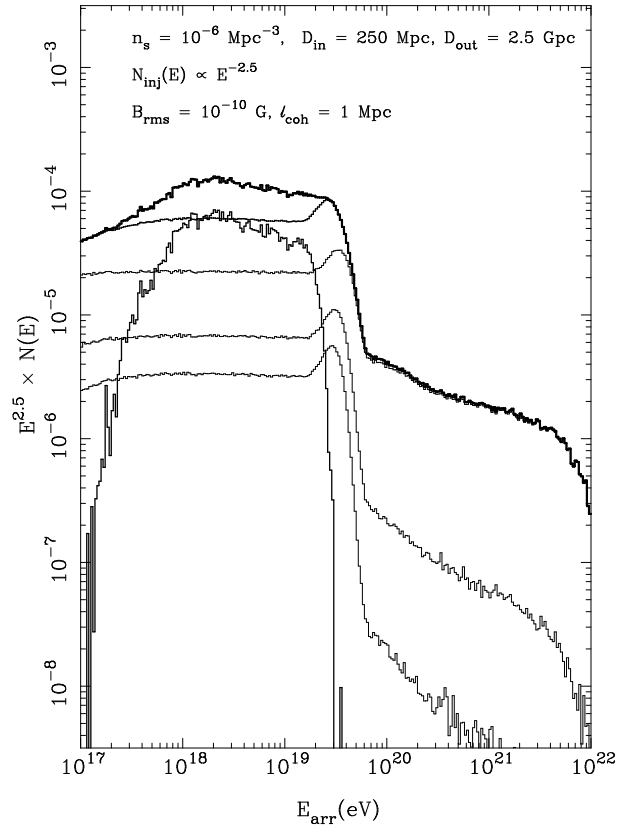


Figure 11. As in figure 10: the UHECR spectrum due to continuous sources with the same source density, $n_s = 10^{-6} \text{ Mpc}^{-3}$, but with a different Monte-Carlo realization of the source distribution within a distance $D_{\text{in}} = 250 \text{ Mpc}$. In this realization there are a few more close sources. This distribution is compatible with existing observations, whereas the spectrum shown in figure 10 is not.

$10^{51} - 10^{52} \text{ erg}$, assuming a conversion efficiency of 10 % into gamma rays.

However, Wijers *et al.* (1998) have pointed out that most GRB formation scenarios, such as neutron star mergers (e.g. Paczyński, 1986; Narayan, Paczyński & Piran, 1992) or hypernovae (Paczyński, 1997) involve the end-product of massive star evolution. One should therefore expect that the GRB rate closely follows, on cosmological timescales, the star formation rate. The latter seems to peak at a larger redshift ($z \gtrsim 2$). This evolving GRB scenario implies a larger distance scale ($z \gtrsim 2$) and total energy yield ($E_{\text{GRB}} \sim 10^{53} \text{ erg}$) for a typical burst, leading to a correspondingly lower burst rate per unit volume in the local ($z \simeq 0$) universe. On the basis of the observed rate of GRBs, Wijers *et al.* estimate a local burst rate equal to:

$$Q_{\text{GRB}}^{\text{ev}} \simeq 10^{-10} \left(\frac{H_0}{75 \text{ km s}^{-1} \text{ Mpc}^{-1}} \right)^{-3} \text{ Mpc}^{-3} \text{ yr}^{-1}. \quad (67)$$

The local burst rate is the relevant quantity for the production of UHECRs, which must originate within a distance D_{max} .

The main uncertainty in these estimates is the unknown beaming factor of the gamma radiation, which could increase

the burst rate significantly above the one derived (from observations) assuming isotropic emission. In the hypernova scenario in particular, where the energy is generated in a short-lived torus around a stellar core that has collapsed into a black hole, beaming could be significant. Finally, given the limited number of events with X-ray, optical and/or radio counterparts for which a distance can be derived, one can at this time not exclude the possibility that both the hypernova and binary merger mechanism produce a population of GRBs.

One can define an (energy-dependent) critical distance $D_b(E)$ which bounds the typical volume within which one expects to find a single source, $N_s(D \leq D_b) = 1$ for given energy E :

$$\int_0^{D_b} 4\pi D^2 Q_{\text{GRB}} t_{\text{del}}(E, D) dD = 1. \quad (68)$$

Using $t_{\text{del}} \propto D^2$ it is easily checked that this corresponds to (Miralda-Escudé & Waxman, 1996)

$$\frac{4\pi}{5} Q_{\text{GRB}} D_b^3 t_{\text{del}}(E, D_b) = 1. \quad (69)$$

Using Eqn. (24) one finds:

$$D_b(E) \simeq 17 \left(\frac{E_{20}}{Z B_{-9}} \right)^{2/5} \ell_0^{-1/5} Q_{-8}^{-1/5} \text{ Mpc}, \quad (70)$$

where $Q_{-8} = Q_{\text{GRB}}/(10^{-8} \text{ Mpc}^{-3} \text{ yr}^{-1})$. Since losses limit the source distance for $E \gtrsim 10^{19.5} \text{ eV}$ to $D \leq D_{\text{max}} \simeq 50 \text{ Mpc}$, one can define an energy E_b such that one expects only one source to contribute to the flux at that energy at any one time. This corresponds to $D_b(E_b) = D_{\text{max}}$ and

$$E_b \simeq 1.6 \times 10^{21} Z B_{-9} Q_{-8}^{1/2} \ell_0^{1/2} \left(\frac{D_{\text{max}}}{50 \text{ Mpc}} \right)^{5/2} \text{ eV}. \quad (71)$$

In terms of D_b and E_b , the number of sources contributing at any time to the UHECR flux from the sphere bounded by D_{max} may be written as (Miralda-Escudé & Waxman, 1996):

$$N_s(E, D \leq D_{\text{max}}) = \left[\frac{D_{\text{max}}}{D_b(E)} \right]^5 = \left[\frac{E}{E_b} \right]^{-2}. \quad (72)$$

The distance $D_b(E)$ (by definition) corresponds to the distance separating the local volume from which the UHECR flux at given E will be intrinsically bursty and the extended volume beyond where the spread in arrival times is large and the fluxes from individual sources overlap, resulting in a quasi-steady UHECR flux at Earth. In a similar way, the energy E_b is the energy above which the UHECR flux should become strongly time-dependent, depending on the chance occurrence of an UHECR production event within a distance $D_b(E)$.

The requirement, implied by observations, that some $N_s \gtrsim 10^2$ independent sources contribute to the UHECR flux above $E_{\text{GZK}} \sim 10^{19.5} \text{ eV}$ corresponds to

$$D_b(10^{19.5} \text{ eV}) \lesssim \frac{D_{\text{max}}}{100^{1/5}} \simeq 20 \left(\frac{D_{\text{max}}}{50 \text{ Mpc}} \right) \text{ Mpc}. \quad (73)$$

This implies a lower limit on B_{rms} , assuming $\ell_{\text{coh}} \simeq 1 \text{ Mpc}$ and protons ($Z = 1$):

$$B_{\text{rms}} \gtrsim 2.0 \times 10^{-10} Q_{-8}^{-1/2} \left(\frac{D_{\text{max}}}{50 \text{ Mpc}} \right)^{-5/2} \text{ G}. \quad (74)$$

In the non-evolving GRB scenario ($Q_{-8} \sim 1$) this is well within the observational constraints on B_{rms} . These estimates correspond to a typical delay time for particles from that volume of order

$$\langle t_{\text{del}} \rangle (10^{19.5} \text{ eV}, D_b) \approx 4.9 \times 10^3 Q_{-8}^{-1} \left(\frac{D_{\text{max}}}{50 \text{ Mpc}} \right)^{-3} \text{ yr}.$$

If the *local* GRB rate per unit volume is indeed as low as proposed by Wijers *et al.* (1998) in an evolving scenario without beaming, $Q_{-8} \sim 10^{-2}$, the random IGM magnetic field would have to be close to the upper limit implied by observations: $B_{\text{rms}} \simeq 10^{-9} \text{ G}$. In that case one has $E_b \simeq 3 \times 10^{20} \text{ eV}$, and the most energetic cosmic ray ever observed ($E \sim 3 \times 10^{20} \text{ eV}$) is right in the energy range separating the quasi-steady flux at lower energies and the intrinsically bursty (intermittent) flux at higher energies.

At energies $E > E_b$, impulsively produced particles arrive in bursts separated by some $2 \times 10^2 Q_{-8}^{-1} \text{ yr}$, with the relative burst duration scaling as $\langle t_{\text{del}} \rangle / \tau(D_{\text{max}}) = [E/E_b]^{-2}$. It is therefore unlikely that many particles will be observed at any time at energies exceeding $\sim 10^{21} \text{ eV}$, with $E \gg E_b$, even if they are produced at the source and survive in transit. This is especially true in the evolving GRB scenario, where $E_b \simeq 1.6 \times 10^{20} B_{-9} \ell_0 \text{ eV}$. Given that some 100 sources contribute to the flux around $10^{19.5} \text{ eV}$, this implies that the flux should become intrinsically bursty at an energy $E_b \simeq 10^{20.5} \text{ eV}$. The observation of a single particle at $3 \times 10^{20} \text{ eV}$ is therefore within the possibilities of this scenario.

Present experiments have too small a collecting area to experimentally check the prediction of a quasi-steady flux below E_b and an intrinsically bursty flux above E_b with a ‘duty cycle’ decaying as E^{-2} . The proposed Auger observatory, which improves the available collection area by more than an order of magnitude, should be able to settle this question.

The effect of the delays on the spectrum from a bursting source is shown in Figures 12, 13 and 14. Figure 12 shows the accumulated arrival spectrum due to a monochromatic burst of particles at $E_{\text{inj}} = 10^{21} \text{ eV}$ for different integration times after the arrival of photons from the same source. Particles at lower energies accumulate a longer delay, leading to a low-energy decline in the spectrum for finite integration time.

Figure 13 shows a similar calculation, but now for a source at a distance of 25 Mpc injecting a power-law spectrum $N(E) \propto E^{-2.5}$. The assumed IGM field has an amplitude $B_{\text{rms}} = 10^{-10} \text{ G}$. Shown are the accumulated particle distributions for integration times of 1, 10, 25 and 50 yr starting immediately after arrival of photons from the same source, and the total arrival spectrum for infinite integration time.

Figure 14 shows the spectrum of particles received in five 20-year intervals from a source 25 Mpc distant, with a power-law injection spectrum $N(E) \propto E^{-2.5}$. These particles propagate through a random field with a field strength $B_r = 10^{-10} \text{ G}$ with a coherence length of $\ell_{\text{coh}} = 1 \text{ Mpc}$. Particles of lower energy are seen with a larger delay, with a fairly narrow spread around the mean arrival energy. The

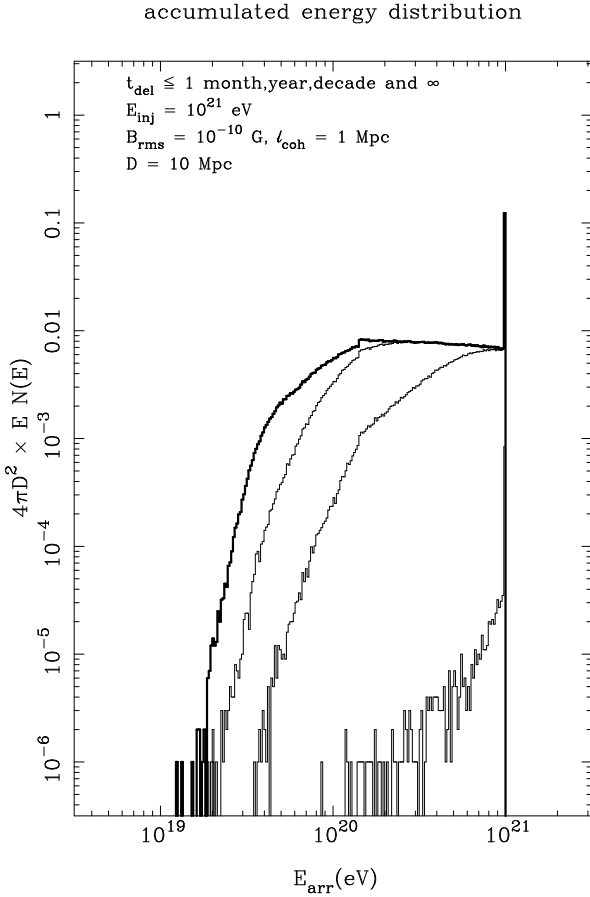


Figure 12. Accumulated particles from a single bursting source at 10 Mpc, as a function of the integration time after photon arrival. The source produces particles at an energy $E_{inj} = 10^{21}$ eV. The assumed intergalactic field has an amplitude $B_{rms} = 10^{-10}$ G. The time $t_{del}(\max)$ ranges from one month to one decade. The thick line is the total arrival distribution $EN(E)$ for $t_{max} \rightarrow \infty$. For finite integration time there is a sharp decline towards low energies due to the strong energy dependence of the delay time, $\langle t_{del} \rangle \propto E^{-2}$. At the injection energy, the expected delay is $t_{del} \simeq 0.3$ year. The finite spread in energy of the particles is due to Poissonian statistics of the photon encounter rate in the photo-pion production process responsible for the energy losses from 10^{21} eV.

spectrum observed at Earth consists of many such contributions from different sources with different delays.

We have simulated arrival spectra that result from a distribution of identical bursting sources which produce particles with an energy distribution $N(E)dE = \kappa E^{-s} dE$. Results are shown for $s = 2.5$. Within a distance $D \leq D_{in} = 100$ Mpc, the source distances are drawn from a distribution satisfying the scaling law (72). In addition we calculate the quasi-steady background from sources with a distance $D > D_{in}$ up to a distance $D_{max} = 2.5$ Gpc. This distance is so large that, for the assumed field strength in the intergalactic medium, no particles reach the observer within a Hubble time from larger distances (see Eqn. 34). The sources at distances $D \leq D_{in}$ are given an ‘age’ with respect to the arrival of photons, distributed uniformly in the range $0 < t < \langle t_{del} \rangle(E, D)$, when UHECR detection starts. Different assumptions about source age have been tried (e.g.

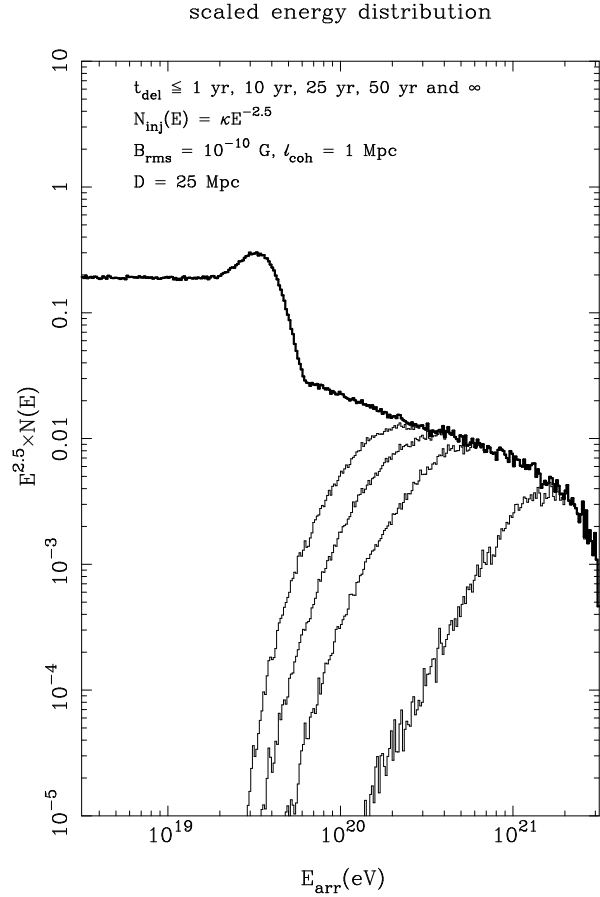


Figure 13. The arrival energy distribution accumulated from a source at 25 Mpc after propagation through a 10^{-10} G random field with correlation length $\ell_{coh} = 1$ Mpc. Particles are injected with a power-law, $N(E) = \kappa E^{-2.5}$. The arrival distribution is multiplied by a factor $\propto E_{arr}^{2.5}$ so that an unmodified source spectrum corresponds to a horizontal line. The integration time ranges from 1 year to 50 year after arrival of photons from the same bursting source. The thick line is the total arrival spectrum after all particles from the source have been received.

$0.5 \langle t_{del} \rangle < t < 1.5 \langle t_{del} \rangle$) but do not lead to significantly different results. The representative energies for determining source distribution and age are chosen logarithmically equidistant, with $E_n = E_b / (\sqrt{2})^{(n-1)}$ and $n = 13$. Figures 15 and 16 show two representative examples of the resultant total spectrum for an assumed field strength $B_{rms} = 10^{-10}$ G. They correspond to two different statistical realizations of the the source distribution for $D \leq D_{in}$. We assumed a GRB rate per unit volume of $Q_{-8} = 1$. At energies below $E_* \sim 10^{17}$ eV, one sees the effect of the transition to spatial diffusion as a decline in the spectrum towards lower energies, as discussed in Section 2.3.

These two examples show that there is a significant ‘tail’ of particles above the GZK cut-off energy. However, the flux in this tail depends sensitively on the observation window. Only a few sources contribute for energies $E \leq E_b$, with the distance distribution $\propto D^5$ strongly favoring the largest possible distances around $D = D_{max}$. As a result, like in the case of continuous sources, the contribution at the highest energies will be dominated by those closest few sources

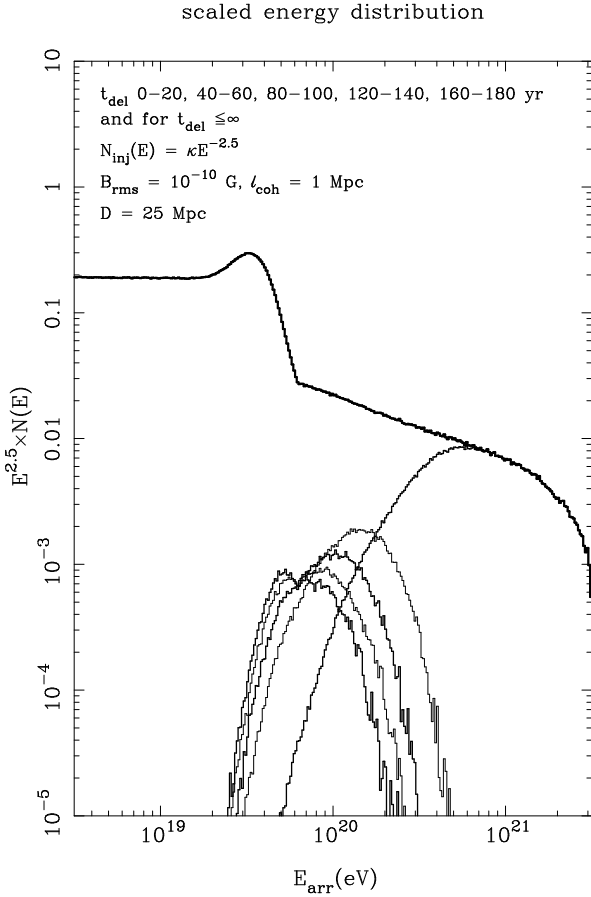


Figure 14. Particles accumulated in five twenty-year intervals, equally spaced in the range $0 < \langle t_{\text{del}} \rangle < 180$ yr, from a single bursting source at a distance of 25 Mpc, after propagation through a random field with field strength of 10^{-10} G and a coherence length $\ell_{\text{coh}} = 1$ Mpc. The injection spectrum is a power-law, $N(E) dE = \kappa E^{-2.5} dE$. The dominant power-law behaviour has been scaled away so that the unmodified source spectrum is a horizontal line. The thickest line is the total arrival spectrum which would be accumulated over a large time interval after the arrival of photons from the same source.

which in addition have burst at the right time for the particles to reach the observer at the present epoch.

6 DISCUSSION

We have considered the propagation of ultra-high-energy cosmic rays in a disordered but space-filling intergalactic magnetic field. We have derived theoretical results for the accumulated deflection angle and time delay as a function of source distance, and compared these with numerical simulations of the random magnetic deflection of UHECRs. Depending on the typical magnetic field strength, the delay for particles originating from a distance of 50 Mpc at 10^{20} eV could range from 10 years for $B = 0.01$ nG to 10^5 years if $B = 1$ nG. We found very good agreement between theory and simulations. We have also shown that *spatial* diffusion due to random magnetic cells does not occur for distances up to 100 Mpc except for particles with energies below $\sim 10^{19} B_{-9}$ eV. Spatial diffusion does limit

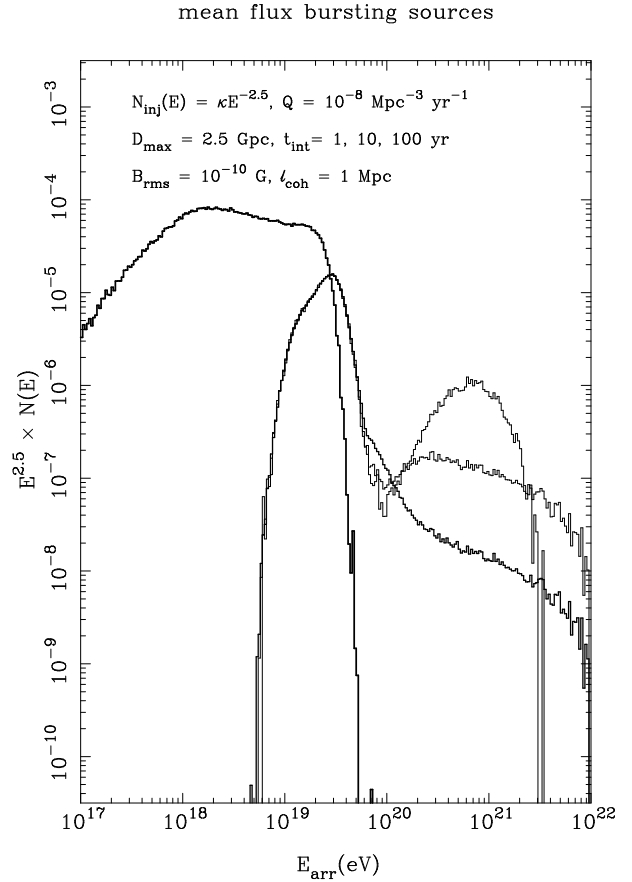


Figure 15. The time-averaged flux $\times E^{2.5}$ due to bursting sources. It is assumed that all sources inject an identical spectrum $N(E) dE \propto E^{-2.5} dE$ for $10^{17} < E < 10^{22}$ eV. The thick line in the range $10^{17} < E_{\text{arr}} < 10^{19.5}$ eV corresponds to the steady background due to sources more distant than 100 Mpc, the burst distance D_b at an energy $E_b \simeq 10^{21}$ eV for the assumed field strength, $B_{\text{rms}} = 10^{-10}$ G. The decline in this contribution below 10^{18} eV is due to the fact that particles undergo spatial diffusion at these energies, and only particles from relatively nearby sources can reach the observer within a Hubble time. The sharp cut-off at $10^{19.5}$ eV in the flux from distant sources is the GZK cut-off due to photo-pion production on the CMWB photons. The high-energy part of the spectrum, which peaks around the GZK cut-off, is due to bursting sources within 100 Mpc. They are distributed according to the $N(\leq D) \propto D^5$ relation. The mean flux is shown for three integration times: $t_{\text{int}} = 1$ (thin line), 10 (thicker line) and 100 year (thickest line). This flux varies considerably above 10^{20} eV.

the background flux from distant sources below the Greisen-Zatsepin-Kuz'min cut-off energy so that the UHECR flux should decay below an energy of $\sim 10^{17} - 10^{18}$ eV as the sampling volume decreases with energy.

We have calculated the arrival spectra which result from the interaction of UHECRs with the photons of the Cosmic Microwave Background Radiation, and demonstrated that a significant flux of particles remains above the Greisen-Zatsepin-Kuz'min cut-off energy $E_c \sim 10^{19.5}$ eV for source distances up to ~ 50 Mpc.

We discussed the implications of impulsive production of UHECRs in gamma-ray bursts, as proposed by Waxman (1995a) and Vietri (1995). We have produced composite

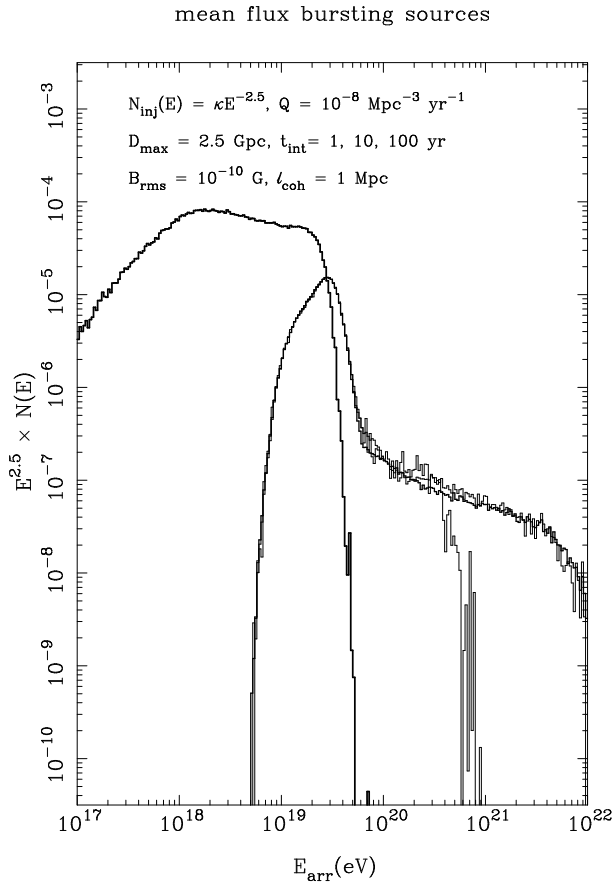


Figure 16. As in figure 15, but with a different Monte Carlo realization of the source distribution $N(\leq D) \propto D^5$ for $D \leq 100$ Mpc.

spectra that demonstrate that, just as in the case of continuous production in powerful radio galaxies, it is likely that the highest energy cosmic rays originate from only a few sources, located at $D \lesssim D_{\max} \simeq 50$ Mpc. These simulations imply that the fact that the GZK cut-off around 3×10^{19} eV is not very pronounced in the observations is probably the result of a few UHECR production events relatively close by. The Poisson statistics of photo-pion production lead to a significant high-energy tail in the particle flux above the GZK cut-off provided enough sources are located within 50 Mpc. The observational fact that UHECRs above the GZK cut-off energy arrive from directions distributed over the whole sky implies, in our view, that the impulsive production scenario is more likely, given the low space density of powerful radio galaxies, which seem to be the only other likely production site of UHECRs except possibly shocks associated with large-scale structure formation in the universe, which are equally sparse. This conclusion of course only holds if UHECRs are hadrons and not some exotic particle that is not subject to a significant energy loss mechanism other than redshift as a result of the universal expansion.

In the scenario of impulsive production in gamma-ray bursts, the fact that ~ 100 events are seen above $10^{19.5}$ eV already puts a lower limit on the IGM magnetic field strength of $B_r \sim 0.1 - 1$ nG, depending on the GRB rate per unit volume. For such a field strength, there should not be a significant flux of cosmic rays arriving from outside

our Galaxy below 10^{17} eV, as slow diffusion does not allow such particles to reach us from distant sources within a Hubble time. Also, the typical energy scale separating the quasi-steady flux at lower energy, due the spread in arrival times, and the intrinsically bursty flux at higher energies is close to that of the highest energy cosmic ray ever observed: $E_b \sim 10^{20.5} - 10^{21.5}$ eV. Our simulations show that the resulting flux at Earth in this scenario is already strongly variable in time at an energy $E \sim 0.2 E_b$. Therefore any interpretation of the observed arrival spectrum in terms of a power-law fit, appropriate for continuous sources, is in our view hazardous at high energies, as is a firm conclusion about the presence (or absence) of a signature of the GZK cut-off in the observed spectrum.

We have made a significant simplification in that we assumed that the IGM magnetic field, although randomly directed with a coherence length in the Mpc range, fills intergalactic space homogeneously. A similar calculation could be done assuming the magnetic field is concentrated mainly in clusters. In that case, one should consider the possibility that the cluster fields are so strong ($B_{cl} \sim 10^{-7} - 10^{-6}$ G, with a possible ordered component), that true spatial diffusion of UHECRs could occur in a cluster for particles up to an energy of $10^{20} - 10^{21}$ eV. This would lead to a cluster-scale leaky box model, where UHECRs are confined to clusters for a significant time (Rachen, *private communication*), analogous to the situation which prevails within the Galaxy for the lower energy cosmic rays. Some calculations along these lines have been performed recently by Sigl, Lemoine and Biermann (1998) for the local supercluster. In that case, most of the UHECRs observed at Earth would be from the local group of galaxies, making the question of the production site even more pressing.

ACKNOWLEDGEMENTS

This research was supported by the NWO-ASTRON foundation, grant nr. 781-71-050, (AA, YG), the Research Center for Theoretical Astrophysics, University of Sydney, Australia (AA) and the European Union through EEC-HCM Contact Nr. ERBCHRX-CT94-0604 and EU-TMR Contract Nr. ERBFMRX-CT98-0168.

REFERENCES

- Achterberg, A. & Krüls, W.M. 1992, A&A, 265, L13.
- Aharonian, F.A. & Cronin, J.W. 1996, Phys. Rev. D 50, 1892.
- Berezinskii, V.S., Grigor'eva, S.I. & Zatsepin, G.T. 1975, Astroph. Space Sc. 36, 3.
- Berezinskii, V.S. & Grigor'eva, S.I. 1988, A&A, 19, 91.
- Berezinskii, V.S., Bulanov, S.V., Dogiel, V.A., Ginzburg, V.L., & Ptuskin, V.S. 1990, *Astrophysics of Cosmic Rays*, North Holland Publ. Co., The Netherlands.
- Biermann, P.L. 1995, Nucl. Phys. B Proc. Suppl. 43, 221
- Bird, D.J. et al. 1994, ApJ, 424, 491.
- Bird, D.J. et al. 1995, ApJ, 441, 144.
- Blumenthal, G.R. 1970, Phys. Rev. D., 1, 1596.
- Chodorowski, M., Zdziarski, A. & Sikora, M. 1992, ApJ, 400, 181.
- Davidson, R.C. 1972, *Methods in Nonlinear Plasma Theory*, Ch. 8, Academic Press, New York.
- de Lapparent, V., Geller, M.J. & Huchra, J.P. 1986, ApJ, 202, L1.

- Djorgovski, S.G. et al. 1997, *Nature*, 387, 876.
 Elbert, J.W. & Sommers, P. 1995, *ApJ*, 441, 151.
 Farrar, G.R. & Biermann, P.L. 1998, *Phys. Rev. Lett.* 81, 3579.
 Gallant, Y.A. & Achterberg, A. 1999, *MNRAS*, 305, L6.
 Gardiner, C.W. 1983, *Handbook of Stochastic Methods*, Springer Verlag, Berlin.
 Greisen, K. 1966, *Phys. Rev. Lett.*, 16, 748.
 Hayashida, N. et al. 1996, *Phys. Rev. Lett.*, 77, 1000.
 Hill, C.T. & Schramm, D.N. 1985, *Phys. Rev. D*, 31, 564.
 Kang, H., Ryu, D. & Jones, T.W. 1996, *ApJ*, 456, 422.
 Kang, H., Rachen, J.P. & Biermann, P.L. 1997, *MNRAS*, 286, 257.
 Kewley, L.J., Clay, R.W. & Dawson, B.R. 1996, *Astrop. Phys.* 5, 69.
 Kulsrud, R.M., Cen, R., Ostriker, J.P. & Ryu, D., 1997, *ApJ*, 480, 481.
 Mannheim, K. & Biermann, P.L. 1989, *A&A*, 221, 211.
 Miralda-Escudé, J. & Waxman, E. 1996, *ApJ*, 462, L59.
 Kronberg, P.P. 1996, *Space. Sc. Rev.*, 75, 387.
 Lesieur, M. 1987, *Turbulence in Fluids*, Kluwer Academic Publ., Dordrecht.
 Metzger, M.R. et al. 1997, *Nature*, 387, 878.
 Milgrom, M. & Usov, V. 1995, *ApJ*, 449, L37.
 Miralda-Escudé, J. & Waxman, E. 1996, *ApJ*, 462, L59.
 Narayan, R., Paczyński, B. & Piran, T., 1992, *ApJ* 395, L83.
 Norman, C.A., Melrose, D.B. & Achterberg, A. 1995, *ApJ*, 454, 60.
 Øksendal, B. 1991, *Stochastic Differential Equations*, third ed., Springer Verlag, Berlin.
 Paczyński, B. 1986, *ApJ*, 308, L43.
 Paczyński, B. 1997, *ApJ*, submitted.
 Rachen, J.P., & Biermann, P.L. 1993, *A&A*, 272, 161.
 Sigl, G., Lemoine, M. & Biermann, P.L. 1998: MPIFR Preprint nr. 774.
 Sigl, G., Schramm, B.N. & Bhattacharjee, P. 1994, *Astrop. Phys.*, 2, 401.
 Stanev, T., Biermann, P.L., Lloyd-Evans, J. & Watson, A.A. 1995, *Phys. Rev. Lett.*, 75, 3056.
 Stepney, S. & Guilbert, P.W. 1983, *MNRAS*, 204, 1269.
 Sturrock, P.A. 1994, *Plasma Physics*, Cambridge Univ. Press, Cambridge, UK, Ch. 18.
 Subramanian, K. & Barrow, J.D. 1998, *Phys. Rev. D*, 58, 083502-1.
 Takeda, M. et al. 1998, *Phys. Rev. Lett.* 81, 1163.
 Taylor, G.I. 1921, *Proc. London Math. Soc.* 20, 196.
 van Paradijs, J. et al. 1997, *Nature*, 386, 686.
 Vietri, M. 1995, *ApJ*, 453, 883.
 Waxman, E. 1995a, *Phys. Rev. Lett.*, 75, 386.
 Waxman, E. 1995b, *ApJ*, 452, L1.
 Waxman, E. & Coppi, P. 1996, *ApJ*, 464, L75.
 Waxman, E. & Miralda-Escudé, J. 1996, *ApJ*, 472, L89.
 Wijers, R.A.J.M., Bloom, J.S., Bagla, J.S. & Natarajan, P. 1998, *MNRAS*, 294, L13.
 Yoshida, S. et al. 1995, *Astropart. Phys.*, 3, 105.
 Yoshida, S. & Teshima, M. 1993, *Prog. Theor. Phys.*, 89, 833.
 Zatsepin, G.T. & Kuz'min, V.A. 1966, *JETP Lett.*, 4, 78.
 Zweibel, E.G. & Heiles, C. 1997, *Nature*, 385, 131.

APPENDIX A: SCATTERING ON A SPECTRUM OF RANDOM FIELDS

We consider the general case of a broad-band spectrum of random turbulent magnetic fields, given by a Fourier expansion of the form

$$\mathbf{B}(\mathbf{x}) = \int \frac{d^3\mathbf{k}}{(2\pi)^3} \tilde{\mathbf{B}}(\mathbf{k}) e^{i\mathbf{k} \cdot \mathbf{x}}, \quad (\text{A1})$$

with $\langle \mathbf{B} \rangle = 0$. For homogeneous isotropic turbulence the Fourier components satisfy the relation

$$\langle \tilde{\mathbf{B}}_i(\mathbf{k}) \tilde{\mathbf{B}}_j(\mathbf{k}') \rangle = \frac{\mathcal{B}(|\mathbf{k}|)}{8\pi k^2} \tilde{P}_{ij} (2\pi)^6 \delta^3(\mathbf{k} + \mathbf{k}'). \quad (\text{A2})$$

Here we have employed the standard random-phase approximation, and defined the projection tensor $\tilde{P}_{ij} = \delta_{ij} - \kappa_i \kappa_j$ in terms of the unit vector $\boldsymbol{\kappa} = \mathbf{k}/|\mathbf{k}|$ which appears because the magnetic field is solenoidal:

$$\boldsymbol{\nabla} \cdot \mathbf{B} = 0 \iff \mathbf{k} \cdot \tilde{\mathbf{B}}(\mathbf{k}) = 0. \quad (\text{A3})$$

The power spectrum $\mathcal{B}(k)$ of the magnetic field has been normalised in such a way that

$$B_{\text{rms}}^2 \equiv \langle |\mathbf{B}|^2 \rangle = \int_0^\infty dk \mathcal{B}(k), \quad (\text{A4})$$

with $k \equiv |\mathbf{k}|$.

The equation of motion (8) for an ultra-relativistic particle yields, by the Kubo-Taylor formula, the following expression for the diffusion coefficient describing the propagation direction change:

$$\mathcal{D}_{ij} \simeq \left(\frac{Ze}{E} \right)^2 \int_0^\infty ds \int dk \int \frac{d\Omega_k}{8\pi} \mathcal{B}(k) Q_{ij} e^{i\mathbf{k} \cdot \hat{\mathbf{n}}s}. \quad (\text{A5})$$

We have employed the quasi-linear approximation where the *unperturbed* motion, $\mathbf{x}(s) = s\hat{\mathbf{n}}$, is used to evaluate the phase factor in the integral. To obtain this expression we have used Eqn. (A2), defined the solid angle $d\Omega_k$ in Fourier space so that $d^3\mathbf{k} = k^2 d\Omega_k dk$, and introduced the tensor

$$Q_{ij} = \delta_{ij} - n_i n_j - (\hat{\mathbf{n}} \times \boldsymbol{\kappa})_i (\hat{\mathbf{n}} \times \boldsymbol{\kappa})_j. \quad (\text{A6})$$

Choosing $\hat{\mathbf{n}} = \mathbf{e}_z$ and defining position angles in Fourier space by

$$\boldsymbol{\kappa} = (\sin \theta \cos \phi, \sin \theta \sin \phi, \cos \theta) \quad (\text{A7})$$

so that $\boldsymbol{\kappa} \cdot \hat{\mathbf{n}} = \cos \theta \equiv \mu$, one can perform the integration over $d\Omega_k = d\phi d\mu$ and s . The integration over ϕ is simple, involving the integral

$$\int_0^{2\pi} d\phi Q_{ij} = 2\pi \left(\frac{1 + \mu^2}{2} \right) (\delta_{ij} - n_i n_j). \quad (\text{A8})$$

The integration over path length s only involves the complex phase factor:

$$\int_0^\infty ds e^{ik\mu s} = \pi \delta(k\mu) = \frac{\pi}{k} \delta(\mu). \quad (\text{A9})$$

The final integration over μ is now trivial, and the resulting expression can be written in the same form as for a collection of randomly oriented magnetic cells,

$$\mathcal{D}_{ij} = \mathcal{D}_0 (\delta_{ij} - n_i n_j), \quad (\text{A10})$$

where the scalar diffusion coefficient \mathcal{D}_0 is given by

$$\mathcal{D}_0 = \frac{\pi}{8} \left(\frac{Ze}{E} \right)^2 \int_{k_{\min}}^\infty dk \frac{\mathcal{B}(k)}{k}. \quad (\text{A11})$$

The low wavenumber cut-off $k_{\min} \sim 2\pi/r_g(E)$ must be introduced since cells with a size exceeding the particle gyration radius will lead to a large-angle deflection in a single cell.

Consider a power spectrum of the form

$$\mathcal{B}(k) = B_0^2 \ell_c \frac{(k\ell_c)^\alpha}{1 + (k\ell_c)^{\alpha+\beta}}, \quad (\text{A12})$$

with $\alpha, \beta > 0$. We assume that $r_g(E) \gg \ell_c$ for simplicity. This spectrum grows as $\mathcal{B}(k) \propto k^\alpha$ for long wavelengths ($k\ell_c \ll 1$), and decays as $\mathcal{B}(k) \propto k^{-\beta}$ at small scales ($k\ell_c \gg 1$). Standard Kolomogorov-type MHD-turbulence, where most energy has been fed into the turbulence at a scale ℓ_c , predicts $\alpha \simeq 4$ and $\beta \simeq 5/3$ (e.g. Lesieur, 1987). Substituting this in Eqn. (A11), one finds

$$\mathcal{D}_0 = \frac{\pi}{8} C_{\alpha\beta} \left(\frac{ZeB_0}{E} \right)^2 \ell_c, \quad (\text{A13})$$

where the constant $C_{\alpha\beta}$ is given by

$$C_{\alpha\beta} = \frac{\pi}{\alpha + \beta} \operatorname{cosec} \left(\frac{\pi\alpha}{\alpha + \beta} \right). \quad (\text{A14})$$

This result is completely analogous with the corresponding expression in the simple case of randomly oriented magnetic cells with identical field strength B_0 , defining the effective coherence length as $\ell_{\text{coh}} = (3\pi C_{\alpha\beta}/4)\ell_c$. For the canonical numbers $\alpha = 4$ and $\beta = 5/3$ one finds $C_{\alpha\beta} \simeq 0.695$ and $\ell_{\text{coh}} \simeq 1.64\ell_c$.

APPENDIX B: DEVIATION ANGLES AND DELAYS

The scattering of UHECRs on randomly oriented magnetic cells can be described as a Stochastic Differential Equation (SDE) of the Itô form (e.g. Øksendal, 1991; Gardiner, 1983). Employing the summation convention in what follows, the stochastic equation of motion for the three components of the unit vector $\hat{n} = (n_1, n_2, n_3)$ along the direction of flight reads:

$$dn_i = -2\mathcal{D}_0 n_i ds + \sqrt{2\mathcal{D}_0} P_{ij}(\hat{n}) dW_j. \quad (\text{B1})$$

Here $P_{ij}(\hat{n}) \equiv \delta_{ij} - n_i n_j$ is the projection tensor onto the plane perpendicular to \hat{n} . This tensor satisfies $\mathbf{P} = \mathbf{P}^\dagger$ and $P_{ij}P_{jk} = P_{ik}$.

The quantity $d\mathbf{W} \equiv (dW_1, dW_2, dW_3)$ is a three-component Wiener process satisfying:

$$\langle dW_i \rangle = 0, \quad \langle dW_i dW_j \rangle = ds \delta_{ij}. \quad (\text{B2})$$

Here the average $\langle \dots \rangle$ denotes an ensemble average which commutes with integration and differentiation with respect to the path length s . The first term in Eqn. (B1) corresponds to ‘dynamical friction’ due to the \hat{n} -dependence of the diffusion tensor, and the second (stochastic) term describes true scattering. Note that the tensor \mathbf{P} projects $d\mathbf{W}$ onto the plane perpendicular to \hat{n} , a property employed in the numerical realization of this process. In the Itô interpretation of SDEs the coefficients in a SDE are *non-anticipating*, i.e. they are independent of the stochastic increments dn_i .

From these definitions one can immediately derive the following relation for the stochastic integrals $n_i(s)$:

$$\frac{d\langle n_i \rangle}{ds} = -2\mathcal{D}_0 \langle n_i \rangle \iff \langle n_i \rangle(s) = \langle n_i \rangle_0 e^{-2\mathcal{D}_0 s}. \quad (\text{B3})$$

We use a subscript 0 to denote initial values at $s = 0$. The Itô rules for two stochastic integrals X and Y (e.g. Øksendal, 1991),

$$d(X \cdot Y) = dX \cdot Y + X \cdot dY + dX \cdot dY, \quad (\text{B4})$$

together with the relations

$$\begin{aligned} (ds)^2 &= 0 \\ dW_i ds &= ds dW_i = 0 \end{aligned} \quad (\text{B5})$$

$$dW_i dW_j = ds \delta_{ij},$$

lead to the following equations:

$$\begin{aligned} d(n_i n_j) &= 2\mathcal{D}_0 (\delta_{ij} - 3 n_i n_j) ds + \\ &+ \sqrt{2\mathcal{D}_0} \{n_i P_{jk} dW_k + (i \rightleftharpoons j)\}. \end{aligned} \quad (\text{B6})$$

Taking an ensemble average one finds an equation for $\langle n_i n_j \rangle$:

$$\frac{d\langle n_i n_j \rangle}{ds} = 2\mathcal{D}_0 \delta_{ij} - 6\mathcal{D}_0 \langle n_i n_j \rangle. \quad (\text{B7})$$

Integration yields

$$\langle n_i n_j \rangle = \langle n_i n_j \rangle_0 e^{-6\mathcal{D}_0 s} + \frac{\delta_{ij}}{3} (1 - e^{-6\mathcal{D}_0 s}). \quad (\text{B8})$$

It is easily checked that these solutions represent diffusion of the direction of flight with diffusion coefficient $\mathcal{D}_{ij} = \mathcal{D}_0 P_{ij}(\hat{n})$. Making a first-order expansion for $\mathcal{D}_0 s \ll 1$, assuming that all members of the ensemble start with the same (statistically sharp) initial conditions n_{i0} , one finds for $\Delta n_i \equiv n_i - \langle n_i \rangle$:

$$\frac{\langle \Delta n_i \Delta n_j \rangle}{2s} \simeq \mathcal{D}_0 (\delta_{ij} - n_{i0} n_{j0}) \equiv \mathcal{D}_{ij}(\hat{n}_0). \quad (\text{B9})$$

Next we consider the the distance integrals along the coordinate axes,

$$x_i(s) = \int_0^s ds' n_i(s'). \quad (\text{B10})$$

Taking the average, using equation (B3), one has

$$\langle x_i \rangle(s) = \frac{n_{i0}}{2\mathcal{D}_0} (1 - e^{-2\mathcal{D}_0 s}). \quad (\text{B11})$$

From the rule (B4), together with $dx_i = n_i ds$, it follows that

$$d(x_i n_j) = (n_i n_j - 2\mathcal{D}_0 x_i n_j) ds + \sqrt{2\mathcal{D}_0} x_i P_{jk} dW_k. \quad (\text{B12})$$

An average yields the differential equation for $\langle x_i n_j \rangle$:

$$\frac{d\langle x_i n_j \rangle}{ds} = \langle n_i n_j \rangle - 2\mathcal{D}_0 \langle x_i n_j \rangle. \quad (\text{B13})$$

Integrating this equation using Eqn. (B8) one finds:

$$\begin{aligned} \langle x_i n_j \rangle(s) &= \frac{\langle n_i n_j \rangle_0 - \frac{1}{3} \delta_{ij}}{4\mathcal{D}_0} e^{-2\mathcal{D}_0 s} (1 - e^{-4\mathcal{D}_0 s}) \\ &+ \frac{\delta_{ij}}{6\mathcal{D}_0} (1 - e^{-2\mathcal{D}_0 s}). \end{aligned} \quad (\text{B14})$$

Note that this expression is symmetric in i and j . In a similar fashion one can derive an equation for $\langle x_i x_j \rangle$:

$$\frac{d\langle x_i x_j \rangle}{ds} = 2 \langle x_i n_j \rangle, \quad (\text{B15})$$

where we used the above symmetry. Direct integration yields:

$$\langle x_i x_j \rangle(s) = \frac{\langle n_i n_j \rangle_0 - \frac{1}{3} \delta_{ij}}{4\mathcal{D}_0^2} \times$$

$$\begin{aligned} & \times \left[1 - e^{-2\mathcal{D}_0 s} - \frac{1}{3} (1 - e^{-6\mathcal{D}_0 s}) \right] \\ & + \frac{\delta_{ij}}{3\mathcal{D}_0} \left[s - \frac{1}{2\mathcal{D}_0} (1 - e^{-2\mathcal{D}_0 s}) \right]. \end{aligned} \quad (\text{B16})$$

These expressions can be used to calculate time delays and deflection angles in the small-angle limit where $\mathcal{D}_0 s \ll 1$. Assuming that all particles start from the origin along the z -axis so that $\hat{\mathbf{n}}(0) = (0, 0, 1)$, one finds the following expressions to first order in \mathcal{D}_0 :

$$\begin{aligned} \langle n_x \rangle &= \langle n_y \rangle = 0, \quad \langle n_z \rangle = 1 - 2\mathcal{D}_0 s; \\ \langle n_x^2 \rangle &= \langle n_y^2 \rangle = 2\mathcal{D}_0 s, \quad \langle n_z^2 \rangle = 1 - 4\mathcal{D}_0 s; \\ \langle x \rangle &= \langle y \rangle = 0, \quad \langle z \rangle = s - \mathcal{D}_0 s^2; \\ \langle x^2 \rangle &= \langle y^2 \rangle = \frac{2}{3} \mathcal{D}_0 s^3, \quad \langle z^2 \rangle = s^2 - 2\mathcal{D}_0 s^3; \\ \langle x n_x \rangle &= \langle y n_y \rangle = \mathcal{D}_0 s^2, \quad \langle z n_z \rangle = s - 3\mathcal{D}_0 s^2. \end{aligned} \quad (\text{B17})$$

The distance r of the particle from the origin follows, for $|x|, |y| \ll |z| \simeq s$, from expanding $r = \sqrt{x^2 + y^2 + z^2}$. To lowest order in $\mathcal{D}_0 s \ll 1$, the resulting average follows from the above expressions:

$$\begin{aligned} \langle r \rangle(s) &\simeq \langle z \rangle + \frac{\langle x^2 \rangle + \langle y^2 \rangle}{2s} \\ &= s - \frac{1}{3} \mathcal{D}_0 s^2. \end{aligned} \quad (\text{B18})$$

This determines the average delay time of charged UHECRs with respect to ballistically propagating particles (photons) originating from the same source at a distance r , to first order in $\mathcal{D}_0 s$:

$$c \langle t_{\text{del}} \rangle \simeq \frac{1}{3} \mathcal{D}_0 r^2. \quad (\text{B19})$$

The unit vector $\hat{\mathbf{r}} = (x, y, z)/r$ along the line of sight from the source to the particle position $\mathbf{r}(s)$ at distance s makes an angle $\theta = \cos^{-1}(z/r)$ with the initial flight direction. For symmetry reasons, assuming isotropic production of particles at the source, one has $\langle \theta \rangle = 0$. The rms value $\theta_{\text{rms}} = \sqrt{\langle \theta^2 \rangle}$ follows from expanding $z/r \simeq 1 - (x^2 + y^2)/2z^2$ together with $\cos \theta \simeq 1 - \frac{1}{2}\theta^2$:

$$\langle \theta^2 \rangle = \frac{\langle x^2 \rangle + \langle y^2 \rangle}{s^2} = \frac{4}{3} \mathcal{D}_0 s. \quad (\text{B20})$$

In a similar fashion, one can calculate the rms angle between the line of sight from the source to the observer and the flight direction from

$$\cos \alpha' \equiv \hat{\mathbf{n}} \cdot \hat{\mathbf{r}} \simeq \frac{n_x x + n_y y + n_z z}{s}. \quad (\text{B21})$$

Expanding the cosine and using the above averages, one finds:

$$\langle \alpha'^2 \rangle = \frac{4}{3} \mathcal{D}_0 s. \quad (\text{B22})$$

This determines the rms angular spread in arrival directions around the direction to the source as measured by an observer at a distance $r \approx s = ct$ from the source.

One can also calculate the long-time behaviour for $\mathcal{D}_0 s \gg 1$. In particular one finds that almost all memory of the initial conditions is lost:

$$\langle n_i \rangle \rightarrow 0, \quad \langle n_i^2 \rangle \rightarrow \frac{1}{3};$$

$$\langle x \rangle = \langle y \rangle = 0, \quad \langle z \rangle \rightarrow \frac{1}{2\mathcal{D}_0}; \quad (\text{B23})$$

$$\langle x_i n_j \rangle \rightarrow \frac{\delta_{ij}}{6\mathcal{D}_0}, \quad \langle x_i x_j \rangle \rightarrow \frac{s}{3\mathcal{D}_0} \delta_{ij}.$$

The last relation corresponds to isotropic *spatial* diffusion, where the distance r to the source increases as

$$\langle r^2 \rangle \simeq \frac{s}{\mathcal{D}_0} \equiv 2\mathcal{K}t, \quad (\text{B24})$$

where the spatial diffusion coefficient is

$$\mathcal{K} \equiv \frac{c}{2\mathcal{D}_0}. \quad (\text{B25})$$

Here we use $s = ct$ for ultra-relativistic particles. The corresponding mean-free-path, defined by $\mathcal{K} = \frac{1}{3}\lambda_{\text{mfp}}c$, is $\lambda_{\text{mfp}} = 3/2\mathcal{D}_0$.